Author Manuscript

Author Manuscript

Author Manuscript

Author Manuscript

HHS Public Access

Author manuscript

Ultrasound Med Biol. Author manuscript; available in PMC 2017 March 01.

Published in final edited form as:

Ultrasound Med Biol. 2016 March ; 42(3): 699–716. doi:10.1016/j.ultrasmedbio.2015.11.002.

QUEST FOR THE VULNERABLE ATHEROMA: CAROTID STENOSIS AND DIAMETRIC STRAIN—A FEASIBILITY STUDY

Canxing Xu[*,1], **Chun Yuan**[*,†], **Edward Stutzman**[‡], **Gador Canton**[†], **Keith A. Comess**[¶,2], and **Kirk W. Beach**[*,†,§]

[*]Department of Bioengineering, University of Washington, Seattle, Washington, USA

[†]Department of Radiology, Vascular Imaging Laboratory, University of Washington, Seattle, Washington, USA

[‡]D. E. Strandness, Jr. Vascular Laboratory, University of Washington Medical Center, Seattle, Washington, USA

[§]Department of Surgery, University of Washington, Seattle, Washington, USA

Abstract

The Bernoulli effect may result in eruption of a vulnerable carotid atheroma, causing a stroke. We measured electrocardiography (ECG)-registered QRS intra-stenotic blood velocity and atheroma strain dynamics in carotid artery walls using ultrasonic tissue Doppler methods, providing displacement and time resolutions of 0.1 μm and 3.7 ms. Of 22 arteries, 1 had a peak systolic velocity (PSV) >280 cm/s, 4 had PSVs between 165 and 280 cm/s and 17 had PSVs <165 cm/s. Eight arteries with PSVs <65 cm/s and 4 of 9 with PSVs between 65 and 165 cm/s had normal systolic diametric expansion (0% and 7%) and corresponding systolic wall thinning. The remaining 10 arteries had abnormal systolic strain dynamics, 2 with diametric reduction (>−0.05 mm), 2 with extreme wall expansion (>0.1 mm), 2 with extreme wall thinning (>−0.1 mm) and 4 with combinations. Decreases in systolic diameter and/or extreme systolic arterial wall thickening may indicate imminent atheroma rupture.

Keywords

Carotid; Atherosclerosis; Atheroma; Vulnerable plaque; Vasa plaquorum; Vasa vasorum; Strain; Tissue Doppler

INTRODUCTION

The purposes of this study were to: (i) identify carotid artery segments with luminal paradoxical pulsation (systolic peri-stenotic diameter reduction) and (ii) differentiate regions

This is an open access article under the CC BY-NC-ND license (http://creativecommons.org/licenses/by-nc-nd/4.0/).

Address correspondence to: Kirk W. Beach, Emeritus, Surgery and Bioengineering, UW, Ty Gwyn, Kiln Road, Abergavenny, Wales, NP7 9NE, UK. kwbeach@usa.net.

[¶]Retired

[1]Present Address: Zonare Medical Systems, Mountain View, CA, USA.

[2]Present Address: Retired, Portland Oregon, USA.

Author Manuscript Author Manuscript Author Manuscript Author Manuscript

of the arterial wall that exhibit compressible strain indicating the presence of pathologic neovascular vasa vasorum and vasa plaquorum. We postulate that: (i) carotid arterial atheromas are not incompressible, but instead include a dynamic, composite neovascular tissue allowing for intra-atheroma vascular volume changes during periods of adverse transmural pressure, and (ii) these neovascular regions are vulnerable to rupture (Feinstein 2006; Lal et al. 2011; Sun 2014). This transcutaneous ultrasound method for differentiating vulnerable from benign carotid atheromas might allow appropriate, in-time, targeted, prophylactic carotid revascularization therapy.

Atheroma rupture is rare, even in the presence of severe carotid stenosis; only 17% of symptomatic patients and 2% of asymptomatic patients with treatable carotid stenosis experience recognizable motor, sensory, or functional symptoms of stroke attributable to the stenosis within 2 y of detection (De Fabritiis et al. 2002) if not revascularizd. In the patients at highest risk, only 2% per year have a stroke (Gardin et al. 2014). In addition to symptomatic stroke, athero-emboli released by atheroma rupture (Bazan et al. 2014a) may stream to other portions of the cerebral cortex causing “silent” infarcts, effects of which are often attributed to aging and dementia rather than embolic infarction.

Clinical studies of carotid therapies to prevent stroke are further hindered by difficulties inherent in differentiating events caused by carotid athero-emboli from those caused by thrombo-emboli from sub-aortic sources and athero-emboli from intracranial sources (Derdeyn et al. 2014). Even after revascularization and the exclusion of peri-treatment events, nearly 2% of cases have ipsilateral stroke within 4 y (Bonati et al. 2015; Brott et al. 2010). Intra-atheroma hemorrhage is thought to be an initiating and contributing factor to atheroma rupture leading to intra-arterial emboli (Treiman et al. 2015).

We hypothesized that intra-stenotic pressure alterations are required to initiate the process of atheroma rupture. Changes in intra-arterial flow dynamics result from Bernoulli pressure depression effects produced by atherosclerotic pathology. The presence of intra-atheroma hemorrhage was associated with intra-stenotic velocities greater than 4 m/s measured in pre-surgical examination (Beach et al. 1993). At velocities of 4 m/s, the resulting intra-stenotic pressure depression would exceed 64 mm Hg during systole ($\Delta P = 4V_{max}^2$). Such velocities are more likely if collateral blood flow pathways via the circle of Willis are absent (Lal et al. 2011). We postulated that pressure depression .64 mm Hg resulting from intra-vascular atherosclerotic pathology, when combined with a pulse pressure of 40 mm Hg (*i.e.*, BP = 120/80), would cause paradoxical (inverted) intra-stenotic pressure pulsation ($BP_{stenosis}$ = 56/64), a potential harbinger of atheroma eruption. Diametric reduction during systole in severe carotid stenosis has been reported (Bonnefous et al. 2000) and attributed to the Venturi effect (Ramnarine et al. 2003).

Some investigators have used mechanical properties of excised tissue and the stress applied to the atheroma by arterial lumen pressure fluctuations to compute atheroma dynamics. These studies have assumed either linear or non-linear, elastic or plastic tissue properties, but all have considered the tissues to be incompressible (Teng et al. 2014). Other studies of carotid atherosclerosis have compared the presence and characteristics of carotid atheromas with the rate of subsequent stroke or carotid atheroma progression (Nicolaides et al. 2010;

Author Manuscript Author Manuscript Author Manuscript Author Manuscript

Truijman et al. 2014) or past events (van Lammeren et al. 2012). An extreme atheroma expansion event, which may occur when hypertension, arrhythmia and cerebral vasodilation coincide, could lead to atheroma disruption resulting in stroke (Folts 2007).

The vasa vasorum (vasa plaquorum) microvasculature in the atheromatous wall provides a means for the volume of the wall to be changed within each cardiac cycle by the inflow and outflow of blood via the adventitia. The purpose of this study was to measure the dynamic waveform of those volume changes to characterize the pathologic nutritional circulation of the atheroma that may make the atheroma vulnerable to rupture. In addition, we found that in some arteries with high velocity, a paradoxical diametric pulsation (referenced to electrocardiography [ECG]-registered QRS timing) may indicate intimal pressure depression that might facilitate the rupture of the atheroma.

METHODS

Patients scheduled for clinically indicated ultrasound examination of the carotid arteries at the University of Washington Vascular Laboratory were invited to participate in this study. The protocol was approved by the Human Patients Division's institutional review board. Each participating patient signed an approved consent form. No demographic data were gathered; such data were not considered essential to the study hypotheses at the time.

A customized ultrasonic Duplex scanner (Hitachi Hi Vision 5500 system Hitachi Medical System America, Twinsburg, OH, USA) with an EUP-L53 linear-array transducer centered at 7.5 MHz was used to capture three types of data (Fig. 1) from each carotid artery examined, including: (i) one 40-mm-wide 2-D brightness-mode (B-mode) pilot image (Fig. 2); (ii) between 6 and 10 blood Doppler spectral waveforms with simultaneous ECG; and (iii) between 2 and 8 2-D radiofrequency (RF) image panel (6.5-mm-wide) real-time sequences at 270 frames per second using ECG-QRS triggering for tissue Doppler strain data. The 2-D B-mode pilot image was used for anatomic identification and relative spatial registration of the blood Doppler and tissue Doppler data. The ECG-registered QRS complex was used to index the beginning of all time traces, providing temporal alignment within the cardiac cycle. B-Mode, Doppler waveform and RF image panel sequences were acquired sequentially, each involving a different series of cardiac cycles. Therefore, although the first cardiac systole was relatively time registered for analysis, the second displayed cycle often exhibited unavoidable jitter due to natural changes in the QRS-QRS interval during the examination.

Each 2-D RF data panel was captured at a frame rate of 270 Hz beginning at the ECG-QRS trigger and extending for two cardiac cycles. The first frame of the panel series was rendered as a 2-D B-mode image for post-examination manual tracing of arterial wall boundaries. This image was also used to estimate the location of acquisition on the pilot image. The sonographer traced the superficial and deep adventitial and luminal boundaries—$W_1(0)$, $W_2(0)$, $W_3(0)$, $W_4(0)$—on the first frame B-mode image of each panel series (W_1 is the superficial adventitial boundary, W_2 is the superficial intimal wall, W_3 is the deep intimal wall, W_4 is the deep adventitial boundary). These tracings were used as the key locations for RF tracking of the four boundaries in the depth. The autocorrelation method of Rabben et al.

Author Manuscript Author Manuscript Author Manuscript Author Manuscript

(2002) with center frequency correction was used to create a time series, $W_i(t)$, for each beam line from each boundary in each panel series (position vs. time) (Fig. 3a) based on an integration of the frame-to-frame displacement (Shamdasani and Kim 2004). The inter-frame displacements were averaged to provide a velocity for each interface for display: $W_i(t + j) - W_i(t)$, j = 3.7 ms (Fig. 3b). The dimensional change waveforms from interface differences were computed for the diametric waveform $D(t)$, near wall $N(t)$ and far wall $F(t)$, as well as the deviation of the artery center, $C(t)$ (Fig. 3c):

$$D(t) = W_3(t) - W_2(t) - D(0) \quad (1a)$$

$$N(t) = W_2(t) - W_1(t) - N(0) \quad (1b)$$

$$F(t) = W_4(t) - W_3(t) - F(0) \quad (1c)$$

$$C(t) = \left(\frac{[W_3(t) + W_2(t)]}{2}\right) - C(0) \quad (1d)$$

The method of Rabben et al. (2002) with center frequency correction is valid within the coherence interval of the echo. The coherence interval is approximately the coherence length ($L = C/\Delta F$, where ΔF is system bandwidth, and C is the speed of ultrasound in tissue), but extended in length if the echogenic tissue has a strong interface and diminished in time if the echogenic tissue moves laterally out of the sample volume.

In our application, the measured image depth resolution was 0.27 mm (equivalent to the coherence length); the measured lateral image resolution was 0.81 mm, but the displacement data were averaged over the 6.5-mm panel width. The displacement resolution was 0.0001 mm; the largest displacement between frames was 0.0336 mm; the largest overall interface displacement was 0.91 mm. Because the interval displacement was integrated in time to achieve the overall displacement and the fractional interval displacement (0.0336/0.27 = 12%) was small, confidence in measurement accuracy was established. Out-of-beam displacement should be similar to depth displacement (Zahnd et al. 2011), preserving coherence. These constraints also apply to the antecedent methods of tracking tissue motions (Bonnefous et al. 2000, Hoeks et al. 1985; 1990; Hokanson et al. 1972).

The Doppler angle-adjusted systolic and diastolic velocities were computed for all images with a Doppler examination angle less than 65°. The artery was characterized by the highest peak systolic Doppler value of the measurements along the artery.

If the wall is incompressible, the wall area (circumference × thickness) is constant, assuming no longitudinal movement of material; as the diameter (and circumference) increases, the wall thickness would decrease in proportion to the initial thickness divided by diameter. For ease of clinical interpretation in Figure 4, the wall thickness waveforms were scaled using the assumption of constant wall tissue volume:

Author Manuscript Author Manuscript Author Manuscript Author Manuscript

$$S(t) = -\frac{[W_4[0] - W_1[0]]}{N(0)} \times N(t) \quad (2a)$$

$$L(t) = -\frac{[W_4[0] - W_1[0]]}{F(0)} \times F(t) \quad (2b)$$

where $S(t)$ is the near wall, and $L(t)$ is the far wall.

MATLAB software (The MathWorks, Natick, MA, USA) was used to convert the RF ultrasound echo signals to waveforms (Fig. 3a); Microsoft Excel (Redmond, WA, USA) was used for tabulations and graphic displays.

Based on empirical observation of the data, the time-average luminal diametric change during the interval between 150 and 350 ms after QRS was computed to identify systolic diametric reduction; a decrease in diameter exceeding 0.05 mm was classified as systolic diametric reduction (10% of lumen measurements were classified as systolic diametric reduction). Scaled wall thickness changes were compared with diameter changes. Many wall thickness changes were larger than expected from the scaled diameter changes; an unscaled threshold of 0.1 mm was selected empirically as the threshold to identify extreme wall thickness changes, for both increases and decreases (10% of walls were classified as extreme thickness changes).

RESULTS

A total of 22 carotid arteries were examined, and 165 Doppler spectral waveforms and 119 strain panels were obtained and analyzed. From the spectral waveforms acquired at angles less than 65°, the highest angle-adjusted peak systolic Doppler velocity was selected for each artery to classify the stenosis. The velocities ranged from 36 to 363 cm/s, with diastolic velocities from 10 to 122 cm/s (Fig. 5). Only 1 artery had velocities indicating severe stenosis (>70% diameter reduction, PSV >280 cm/s), 4 had intermediate stenosis (50%–69%, PSV between 165 and 280 cm/s), 17 had velocities indicating no severe stenosis (PSV <165 cm/s) (Beach et al. 2012). Systolic and diastolic blood pressures were not measured, so the pulse pressure is not known. However, average pulse pressure for a general population is 51 mm Hg (Pastor-Barriuso et al. 2003); minimum normal is 25 mm Hg; and the range is 20 to 85 mm Hg (Bimenya et al. 2005).

Two alternative methods of counting cases were used: (i) number of arteries, (ii) number of measured panels. Because not all atheromas progress and not all rupture, it can be presumed that each atheroma has an “independent history,” even if exposed to similar factors within a single patient. Therefore, the relationship between wall thickness and wall expansion in separate arterial segments is important, and the associated variables have important relationships, even when taken from the same artery. However, case count is only important when computing *p* values. In this feasibility study with few cases, no *p* values were computed. For each artery, the highest velocities and most extreme displacement measurements were used to characterize the artery behavior of each artery.

Author Manuscript Author Manuscript Author Manuscript Author Manuscript

Figure 5 illustrates the Bernoulli systolic and diastolic pressure depression for the corresponding velocities as orange, blue, pink and purple stripes. For the patient with systolic blood velocity 363 cm/s and diastolic velocity 122 cm/s, the Bernoulli pressure depression is (53 mm Hg) − (6 mm Hg), or 47 mm Hg. This value is centered in the *blue stripe*, 40–50 mm Hg. If this patient has a pulse pressure near the population average (51 mm Hg), then the depressed stenotic pulse pressure is +4 mm Hg higher during systole than diastole. This should reduce the diametric pulse amplitude to near zero, but this case exhibits an inverted pulsation, with diameter decreasing during systole (indicated by the *green triangle*), suggesting that the intra-stenotic pulse pressure is negative. The intra-stenotic pulse pressure might be negative for three possible reasons: (i) the actual systolic intra-stenotic blood velocity is higher than computed by the Doppler equation; (ii) the curvature factor should be added to the conventional Bernoulli equation; (iii) the pulse pressure in this patient is below the population average.

Most of the luminal diametric waveforms (100/119 = 84%) exhibited normal systolic expansion. One luminal expansion was >0.5 mm (Fig. 4c), consistent with tortuosity. In that same region, both the superficial and the deep walls also exhibited large increases in thickness rather than the expected decrease. A minority of the diametric waveforms (8/119 = 7%) were inverted, indicating systolic luminal diametric reduction in five arteries (*green triangles*, Fig. 5). The wall thickness decreased normally during systole in nearly half of the measured walls (113/238 = 47%). Extreme thinning of the artery wall (>0.1 mm) occurred in eight panels involving 5 arteries (Fig. 5, *red diamonds*), 3 of the 5 arteries had velocities >165 cm/s. All of the arteries with peak systolic blood velocity >165 cm/s exhibited luminal diametric reduction (4/5) and/or wall expansion (2/5) (Fig. 5). Of the 9 arteries with intermediate systolic velocities (65 cm/s <*V*<165 cm/s), 1 of 9 exhibited diametric reduction. All arteries with PSVs <65 cm/s and 4 of 9 with PSVs between 65 and 165 cm/s exhibited normal diametric and wall thickness waveforms.

DISCUSSION

In the normal arterial wall, pressure increases from the ambient level (at the adventitial surface) through an intermediate value (at the adventitia–media interface) to luminal pressure at the intima–blood interface (Fig. 6). The transmural pressure profile varies between the systolic (*brown curve*) and diastolic (*blue curve*) profiles during the cardiac cycle. The vasa vasorum penetrate through the adventitia; the vasa arteriolum pressure is near 100 mm Hg (Maurice et al. 1998) and the vasa venolum pressure is near 10 mm Hg (Teng et al. 2012). During diastole, when the adventitial pressure is lowest, blood can enter the entire vasa vasorum network; as the pressure rises toward systolic values, the blood is expressed via the vasa venolum in a process similar to the filling and emptying of the myocardial microcirculation (Ashikawa et al. 1986).

Figure 7a illustrates the hypothetical evolution of an atheroma. The normal carotid intima–media thickness (IMT) is <1 mm, increasing with carotid, coronary and peripheral atherosclerosis (Burke et al. 1995) to a maximum thickness <2 mm.

Author Manuscript Author Manuscript Author Manuscript Author Manuscript

As the atheroma expands, two changes occur: (i) the development of neovascularization in the atheroma (Coli et al. 2008; Giannoni et al. 2009; Papaioannou et al. 2009) and (ii) compensatory remodeling of the adventitia to maintain the normal lumen diameter (Glagov et al. 1987; Yoshida et al. 2015). When the atheroma occupies ~40% of the vessel cross-sectional area (embracing the luminal circumference), compensatory remodeling ceases (Zarins et al. 1988): then progressive atheroma expansion impinges on the lumen, resulting in increasing severity of stenosis. As the atheroma impinges on the carotid lumen, a stenosis becomes “hemodynamically significant” if: (1) collateral pathways are available allowing blood flow to the brain via alternate routes, (1a) flow reduction occurs without pressure reduction across the stenosis, (1b) intra-stenotic high velocities do no occur; (2) no collateral pathways are available, (2a) flow is maintained by brain vasodilation, (2b) resulting in high systolic velocities and (2c) post-stenotic turbulence associated with bruit which dissipates flow energy causing a pressure drop across the stenosis, (2d) cerebral vasodilation increases flow rate in diastole, and (2e) distal tissues exhibit a pulse delay (Lal et al. 2011).

The expected waveforms from the lumen diameter and the superficial and deep vessel walls are provided in Figure 7b. During the cardiac cycle, the normal artery diameter expands in systole as pressure increases and relaxes in diastole (Fig. 7b, left, *red waveforms*). Assuming that the media is incompressible, the constant volume circumferential media decreases in thickness during systole in proportion to the increase in circumference (*green waveforms*), because area (circumference × thickness) is constant. The change in wall thickness with time is inversely proportional to the change in diameter with time. This decrease in medial thickness occurs symmetrically in both the superficial and deep walls in normal arteries (*green waveforms*, left). However, the walls containing neovascular media exhibit various degrees of expansion superimposed on the wall-thinning waveform, providing an alteration in the waveform (*brown waveforms*). When the vasa plaquorum invades the media at the time of atheroma initiation (Galis and Lessner 2009), because the pressure in the vasa arteriolum is ~100 mm Hg (Maurice et al. 1998), the intra-media vasa arteriolum begin to expand (*brown waveform* in center lower row), adding to the medial volume change. As the volume fraction of vasa arteriolum and venolum increases as a result of atheroma growth (Fig. 7b, right), the net pulsation of the wall thickness differs further from the incompressible waveform. Because the atheroma is not axisymmetric, the waveform of the neovascular superficial wall is usually different from the waveform of the neovascular deep wall.

As the vessel lumen becomes stenotic (Fig. 7, right) and the intra-stenotic velocity increases, causing Bernoulli pressure depression, the adverse vasa plaquorum transmural pressure will exacerbate systolic atheroma expansion. The Bernoulli pressure depression (Lima et al. 1983) is proportional to the square of the luminal velocity:

$$\Delta P_b = 4\left(\frac{\mathrm{mmHg}}{\left[(m/s)^2\right]}\right) \times V^2 \quad (3a)$$

where ΔP_b is the pressure reduction at the atheroma surface from the arterial blood pressure (mm Hg), and V is the intra-stenotic velocity (m/s). If the artery is curved, the intimal

Author Manuscript Author Manuscript Author Manuscript Author Manuscript

pressure along the inside of the curvature is also depressed by inertial forces (ΔP_i) (de Andrade 2014; Feng et al. 2014; Shapiro 1962). The estimated magnitude of the depression is similar to the Bernoulli value:

$$\Delta P_i = 8\left(\frac{r}{R}\right) \times \left(\frac{\mathrm{mmHg}}{\left[(m/s)^2\right]}\right) \times V^2 \quad (3b)$$

where r is the radius of the artery, and R is the radius of the bend. For a straight artery, $1/R$ equals zero, and ΔP_i equals zero. Geometry limits the value of $r/R < 1$, but the simplifying assumptions are not valid for $r/R > 0.5$ so the inertial pressure depression effect of curvature is not greater than the Bernoulli effect, but the two values are additive. Computational methods provide a similar, but more detailed result (Wang and Li 2011).

The purpose of this study was to determine that systolic diameter reduction could be measured using non-invasive, transcutaneous ultrasound in atherosclerotic artery walls and that measurements of arterial wall thickness waveforms can provide results that are inconsistent with the assumption of incompressible tissue. Although others have independently resolved the motions of the adventitia and intima (Bazan et al. 2014b) and stenosis diameter (Bonnefous et al. 2000, Ramnarine et al. 2003), or combined the vector blood velocities in the lumen with the vector tissue velocities of the artery wall (Ekroll et al. 2013), the method has not been applied systematically *in vivo* in carotid arteries to measure wall expansion due to atheroma neovascularization. Our study applies the artery wall measurements to atheromas and regions of increased wall thickness to explore their dynamics during different phases of the cardiac cycle.

Systolic diametric reduction and systolic medial expansion might be markers that indicate that the neovascular atheroma is potentially vulnerable to rupture (Redgrave et al. 2008). These markers are indicated by diametric and scaled wall thickness waveforms (Fig. 4) that deviate below the origin line during the systolic period, 150 to 350 ms after the QRS complex. Motion of the arterial axis might also be useful. Bazan et al. (2014b-Fig. 5) reported synchronous pulsatile motions of both superficial and deep adventitial and intimal walls of 0.25 mm. For instance, at 2 s, all of the traces are displaced to the right; at 7 s, all of the traces are displaced to the left. This indicates the primary motion mode is cross-axial displacement, rather than diameter expansion at 2 Hz in their experimental setup. A pulsatile expansion would be indicated by the anterior wall moving left while the posterior wall moved right. The differentiation of cross-axial from vessel diameter pulsation is crucial to understanding atheroma dynamics.

Figure 4a illustrates normal arterial dynamics, which occurred in all eight arteries with low systolic blood velocities and in more proximal normal segments of arteries with more distal stenosis. These waveforms show the onset of normal luminal expansion and normal wall thinning at 42 milliseconds after the QRS, with the onset of the blood velocity upslope at 74 ms and peak systolic blood velocity at 113 ms, long before the lumen reaches maximum diameter at 290 ms. A dicrotic wave at 340 ms appears in the blood velocity, wall thickness and luminal diameter waveforms providing confidence in the validity of the measurement.

Author Manuscript Author Manuscript Author Manuscript Author Manuscript

In this study, only 1 of 22 cases had a systolic blood velocity >280 cm/s, and 4 had peak systolic velocities between 165 and 280 cm/s. For patients screened for carotid stenosis, this distribution is not unusual. In CREST, 6% of carotid stenosis cases had systolic blood velocities >600 cm/s; 1.5% had systolic blood velocities >700 cm/s (Zierler et al. 2014). Although 165 cm/s causes a Bernoulli pressure depression of 10 mm Hg, 360 cm/s causes a pressure depression >50 mm Hg, and 700 cm/s results in a 196 mm Hg pressure depression, which may induce atheroma instability. Of course, such high velocities cannot occur without systolic hypertension and the absence of collateral pathways.

Measurement of blood pressure is not a standard practice during routine clinical examination of the carotid arteries. Asymmetric impingement on the lumen and arterial tortuosity can nearly double the pressure depression on the inside wall of the resulting arterial curve. These luminal hemodynamic forces would be expected to cause distortions in the artery cross section and strain on impinging atheromas, especially when a liquid lipid or hemorrhagic/neovascular core is present (Shaw 1960).

In this study, distortions were found at systolic blood velocities as low as 65 cm/s. This result is surprising because of the relatively low regional pressure changes expected from the Bernoulli equation (eqn 3a). The causes of these distortions are other sources of hemodynamic luminal pressure depression such as wall pressure modulations caused by luminal curvature rather than in measurement error or arterial muscular action.

We use the term *atheroma* rather than *plaque* to emphasize the concept of a vascularized mass rather than a marginal “shield.” The arterial walls are muscular composite materials perforated by arterioles and venules, connected by capillaries. As in other tissues, on the average, these 10-μm-diameter microvessels are arranged in segments 100 μm long spaced at intervals of 100 μm (Hlatky et al. 2002); when inflated, the venules constitute about 4% of the tissue volume. The microvascular spacing varies from 20 μm (Martini and Honig 1969) to 300 μm (Awwad et al. 1986) depending on the metabolic demands of the tissue. The microvascular structures are much smaller than the resolution of transcutaneous imaging systems, requiring alternative approaches to evaluation.

Although the presence of intra-plaque hemorrhage is related to an increased chance of carotid athero-embolic symptoms (McCarthy et al. 1999), the differentiation between static hemorrhage outside the vascular space (Underhill et al. 2010) and intravascular flowing blood in the atheroma microvasculature (Kerwin et al. 2008) may be of greater importance. In this report, only the intravascular volume contributes to pulsatile atheroma volume change. The fractional volume of neovasculature is much larger than the microvasculature of normal tissues (McCarthy et al. 1999).

Arterioles constitute ~1% of tissue volume (Hansen-Smith et al. 1998; Leung et al. 1992), expanding by 10% (0.1% of tissue volume) with each cardiac cycle. Venules can constitute several percent of tissue volume, but because the intraluminal venous pressure is often below the tissue pressure, venules in the artery wall collapse, sustaining intermittent flow (Pedley and Luo 1998; Piechnik et al. 2001; Pihler-Puzovic and Pedley 2014). However, they do have the capacity to inflate as venular luminal pressure exceeds tissue pressure,

Author Manuscript Author Manuscript Author Manuscript Author Manuscript

suddenly increasing tissue volume by several percent (Barendsen and van den Berg 1984). The changes in atheroma volume measured in arterial wall atheromas are likely due to filling of the venular vasa plaquorum.

Although the vasa plaquorum can provide the oxygen needed for atheroma metabolic viability (Buerk and Goldstick 1982), the proliferation of these microvessels may lead to unstable tissue mechanics that render the atheroma vulnerable to rupture. In the normal media, the partial pressure of oxygen reaches a minimum ranging from 10 to 30 mm Hg at a distance of about 0.3 mm from the flowing oxygenated blood (Ritman and Lerman 2007; Schneiderman et al. 1982). The oxygen availability from the vasa arteriolum varies during the cardiac cycle, decreasing in systole as the luminal pressure compresses the deepest extensions of these microvessels. Oxygen availability from the lumen also varies with the cardiac cycle, as well as luminal morphology, with most severe hypoxia during deceleration in regions of flow separation (Back 1976; Back et al. 1977). The need for vasa plaquorum is exacerbated by the higher metabolic demands of the atheroma, nearly double that of normal media (Whereat 1961).

The conversion of intimal thickening to atheroma resembles the growth of other tumors. The thickness of the avascular media (intima–media thickness [IMT]) is less than 2 mm (Allan et al. 1997). This value is consistent with the metabolic requirements of the media (Whereat 1967) and with the finding that an avascular spherical tumor is limited to 3 mm in diameter (Folkman and Hochberg 1973). For a spherical tumor to grow larger, secretion of an angiogenic factor is required (Folkman 1975).

Unlike a spherical tumor in an organ parenchyma with diffusion available along the spherical radii, an atheroma forms in the media which is nearly a plane; nutritional diffusion can only occur along a single dimension from the luminal and adventitial surfaces. An analysis comparing diffusion limits for a uniform metabolizing sphere ($[q/6D] \times (r^2)$, where q is the metabolic rate, D is the diffusion rate and r is the radius) with those for a plane ($[q/2D] \times [\tau^2]$, where τ is the half-thickness) revealed that the Folkman limit for a plane is more than half that for a sphere (1/sqrt[3] ~ 0.58) corresponding to the maximum media thickness in IMT measurements. Thus, like other tumors, an atheroma might be formed from a cell line that secretes an angiogenic factor providing essential nutrition to the atheroma. This is consistent with the observation that atheromas begin from a focal location, then spread both longitudinally and circumferentially from that location in the arterial wall, resulting in eccentric neovascular atheromas. The proliferation of vasa vasorum in atherogenesis is suppressed by anti-angiogenic drugs such as thalidomide (Gossl et al. 2009); thus, the conversion of a stable to a vulnerable atheroma may also be prevented by anti-angiogenic therapy.

The mechanical properties of the arterial wall vary both longitudinally and circumferentially. Although the volume of the avascular media is constant (incompressible), the volume of a neovasculature medial region will vary with inflation and deflation. This arterial wall atheroma strain inflation/deflation hysteresis signature is the hypothesized marker for intra-atheroma “hemorrhage” (Huang et al. 2012) and, thus, for the vulnerable atheroma. This hypothesis is consistent with published evidence: intra-atheroma hemorrhage

Author Manuscript Author Manuscript Author Manuscript Author Manuscript

is associated with symptoms of stroke (Saam et al. 2006; Takaya et al. 2006) and atheroma progression (Takaya et al. 2005). Recent stroke symptoms are associated with atheroma cap rupture (Yuan et al. 2002).

Limitations

In this study, we failed to recruit a large number of cases with severe stenosis and high velocities. We were surprised that the anomalous diametric and wall thickness waveforms were present in cases with moderate systolic velocities, indicating mild stenosis, and even cases with normal arterial velocities. A longitudinal study of cases similar to the study of Takaya et al. (2005) would presumably indicate whether the anomalous waveforms are markers for arteries most likely to develop severe stenosis and/or experience cerebral events (Takaya et al. 2006).

The data acquisition was further limited by:

- The separate acquisitions of 2-D B-mode, spectral Doppler and strain data, which prevented real-time temporal correlation of events
- A limited method for establishing the relative locations of the acquisitions that prevented proper analysis of the spatial relationship between the locations of hemodynamic spectral Doppler and mechanical wall motion measurements
- The lack of vector Doppler data that would provide para-axial blood velocity magnitude for accurate Bernoulli computation
- The lack of multigate vector Doppler providing cross-axial blood oscillatory blood velocity to elucidate impact of the acceleration on the artery walls
- Measurement of tissue motion only perpendicular to the skin in proximity to the radial direction from the artery axis.
- Measurement from only a single plane perpendicular to the skin
- Limited lateral resolution for the radial displacement measurements (Motions within the 6.5-mm-wide panel are not resolved; only the average motion is measured here. But the smallest vascularized atheroma size is 2 mm, so a 2-mm-wide measurement window or smaller is preferred [Fig. 8].)
- Failure to acquire systolic and diastolic blood pressure measurements in both arms before and after the examination
- Failure to acquire information about pressure drop across the stenosis that can be provided by measurements of end-organ pulse waveforms (Kartchner and McRae 1977)

Future enhancements

In addition to radial strain on the atheroma, longitudinal shear exerted by pressure drop also provides potential disrupting forces (Fig. 9). With advanced ultrasound methods, both longitudinal motions of the carotid arteries (Ahlgren et al. 2015) and longitudinal atheroma shear can be measured. The pressure drop waveform exerted on the atheroma cross section

Author Manuscript Author Manuscript Author Manuscript Author Manuscript

will induce shear strains that should also be measured in a complete examination. By using an ultrasound system with a wider aperture, steerable beam pattern and vector Doppler (Dunmire et al. 2000, Ekroll et al. 2014; Lenge et al. 2014; Ricci et al. 2015; Tortoli et al. 2015) for both blood flow and tissue motion, the tissue strains could be oriented to a coordinate system based on the artery axis (Fig. 10) rather than on the ultrasound scanhead face.

Tissue Doppler ultrasound measurements are capable of detecting wall vibrations associated with stenosis (Plett et al. 2001), even in short bursts (Plett and Beach 2005), and measuring wall vibration amplitudes (Sikdar et al. 2005, Sikdar et al. 2007). These vibrations have frequencies up to 500 Hz (Knox et al. 1981; Lees 1984; Lees and Dewey 1970), exceeding the Nyquist limit of this study. Ultrasound can detect these vibrations in small remote arteries (Comess et al. 2011). Although these methods are potentially useful, they do not predict “vulnerable” atheromas.

Advanced ultrasound methods can potentially provide a solution to these problems (Aristizabal et al. 2014; Azar et al. 2012; Chen et al. 2015; Cheung et al. 2012; Ekroll et al. 2014; Housden et al. 2013; Kim et al. 2013; Lenge et al. 2014; Liebgott et al. 2008; Tasinkevych et al. 2013; Zahiri-Azar et al. 2008; Zetting et al. 2014). Although an array of such instruments are described in the literature (Balocco et al. 2010; Ricci et al. 2009; 2014a; 2014b), none focus on identifying and characterizing the pathologic conditions that are theoretically essential to differentiating the vulnerable atheroma from normal. Existing instruments have been validated on phantoms, but phantom models lack important features for evaluating pathology and have not been designed to meet the challenge of differentiating stable from vulnerable atheromas.

To capture the two or three planes of view required to view non-axisymmetric artery diametric reduction, a position locating system monitoring scanhead and patient would be convenient. A key feature might be luminal diametric reduction, which will not necessarily be axisymmetric (Fig. 11). An artery with high internal pressure has a circular cross section. Decreasing internal pressure correlates with a decrease in artery diameter. However, as the internal pressure decreases below the external pressure (adverse [negative] transmural pressure), the lumen becomes elliptical, as the circumferential wall stress vanishes. In this case, the cross-sectional shape is determined by the circumferential wall stiffness and asymmetries in the applied forces.

Alternative approaches to assessing atheroma vulnerability have been considered. For example, magnetic resonance imaging (MRI) has been used to measure vessel wall compliance and blood flow velocity. The dynamic signals used in MRI hemodynamic measurements are acquired from multiple heart beats and, thus, are time-averaged measures. The capabilities of MRI are complementary to those of ultrasound (Table 1). In carotid artery MRI, the reported spatial resolution is 0.8 mm (Zhou et al. 2015). With this resolution and the non-real-time nature of data acquisition, it will be difficult to use MRI to monitor the “atheroma inflation” phenomenon reported here. MRI, however, has two advantages that complement this study: (i) MRI is able to non-invasively characterize atheroma tissues and burden at the carotid bifurcation (Underhill et al. 2010); (ii) contrast-enhanced MRI can

Author Manuscript Author Manuscript Author Manuscript Author Manuscript

quantify atheroma vasa vasorum (Kerwin et al. 2008). These methods may be combined with ultrasound atheroma inflation data to study the relationship of atheroma tissue composition, neovessel formation and their interaction of hemodynamic forces. Furthermore, even though MRI is not able to provide “real-time” measurement of atheroma motion, its ability to measure and track 3-D motion of the vessel wall in the time-averaged manner will still be useful to provide overall vessel motion information to complement the ultrasound information described in this study.

A complete study of pathologic carotid hemodynamics, in addition to direct examination of the atheroma, should also include an indication of the pressure drop across the stenosis. Pulse delay in the end organs such as the eye (Kartchner and McRae 1977; Kartchner et al. 1973) or brain (Kucewicz et al. 2007; 2008) can provide such information, which indicates shear stress on the base of the atheroma.

CONCLUSIONS

Hemodynamic forces on atheromas contribute to atheroma disruption and athero-emboli. This feasibility study has confirmed the potential validity of measuring arterial lumen diametric reduction and demonstrated the potential for measuring abnormal filling of atheroma neovessels using ultrasonic tissue Doppler methods. Such motions might be important markers of vulnerable atheroma.

Acknowledgments

This project was funded in part by National Institutes of Health Award R21 EB006825 (Atherosclerotic Plaque Neovascularization), NIH R01 HL103609 and bequests from Robert W. Beach, Lois M. Enos and Vivian H. Moore.

References

Ahlgren ÅR, Steen S, Segstedt S, Erlöv T, Lindström K, Sjöberg T, Persson HW, Ricci S, Tortoli P, Cinthio M. Profound increase in longitudinal displacements of the porcine carotid artery wall can take place independently of wall shear stress: a continuation report. Ultrasound Med Biol. 2015; 41:1342–1353. [PubMed: 25726134]

Allan PL, Mowbray PI, Lee AJ, Fowkes FG. Relationship between carotid intima-media thickness and symptomatic and asymptomatic peripheral arterial disease. The Edinburgh Artery Study. Stroke. 1997; 28:348–353. [PubMed: 9040688]

Aristizabal S, Amador C, Qiang B, Kinnick RR, Nenadic IZ, Greenleaf JF, Urban MW. Shear wave vibrometry evaluation in transverse isotropic tissue mimicking phantoms and skeletal muscle. Phys Med Biol. 2014; 59:7735–7752. [PubMed: 25419697]

Ashikawa K, Kanatsuka H, Suzuki T, Takishima T. Phasic blood flow velocity pattern in epimyocardial microvessels in the beating canine left ventricle. Circ Res. 1986; 59:704–711. [PubMed: 3815760]

Awwad HK, el Naggar M, Mocktar N, Barsoum M. Intercapillary distance measurement as an indicator of hypoxia in carcinoma of the cervix uteri. Int J Radiat Oncol Biol Phys. 1986; 12:1329–1333. [PubMed: 3759554]

Azar RZ, Dickie K, Pelissier L. Real-time 1-D/2-D transient elastography on a standard ultrasound scanner using mechanically induced vibration. IEEE Trans Ultrason Ferroelectr Freq Control. 2012; 59:2167–2177. [PubMed: 23143567]

Back LH. Analysis of oxygen transport in the avascular region of arteries. Math Biosci. 1976; 31:285–306.

Author Manuscript Author Manuscript Author Manuscript Author Manuscript

Back LH, Radbill JR, Crawford DW. Analysis of oxygen transport from pulsatile, viscous blood flow to diseased coronary arteries of man. J Biomech. 1977; 10:763–774. [PubMed: 606722]

Balocco S, Basset O, Courbebaisse G, Boni E, Frangi AF, Tortoli P, Cachard C. Estimation of the viscoelastic properties of vessel walls using a computational model and Doppler ultrasound. Phys Med Biol. 2010; 55:3557–3575. [PubMed: 20508319]

Barendsen GJ, van den Berg JW. Venous capacity, venous refill time and the effectiveness of the calf muscle pump in normal subjects. Angiology. 1984; 35:163–172. [PubMed: 6703406]

Bazan HA, Smith TA, Donovan MJ, Sternbergh WC. Future management of carotid stenosis: Role of urgent carotid interventions in the acutely symptomatic carotid patient and best medical therapy for asymptomatic carotid disease. Ochsner J. 2014a; 14:608–615. [PubMed: 25598726]

Bazan I, Negreira C, Ramos A, Brum J, Ramirez A. A new high-resolution spectral approach to noninvasively evaluate wall deformations in arteries. Comput Math Methods Med. 2014b; 2014:606202. [PubMed: 24688596]

Beach KW, Hatsukami T, Detmer PR, Primozich JF, Ferguson MS, Gordon D, Alpers CE, Burns DH, Thackray BD, Strandness DE Jr. Carotid artery intraplaque hemorrhage and stenotic velocity. Stroke. 1993; 24:314–319. [PubMed: 8421835]

Beach KW, Leotta DF, Zierler RE. Carotid Doppler Velocity measurements and anatomic stenosis: Correlation is futile. Vasc Endovasc Surg. 2012; 46:466–474.

Biasi GM, Sampaolo A, Mingazzini P, De Amicis P, El-Barghouty N, Nicolaides AN. Computer analysis of ultrasonic plaque echolucency in identifying high risk carotid bifurcation lesions. Eur J Vasc Endovasc Surg. 1999; 17:476–479. [PubMed: 10375482]

Bimenya GS, Byarugaba W, Kalungi S, Mayito J, Mugabe K, Makabayi R, Ayebare E, Wanzira H, Muhame M. Blood pressure profiles among Makerere University undergraduate students. Afr Health Sci. 2005; 5:99–106. [PubMed: 16006215]

Bonati LH, Dobson J, Featherstone RL, Ederle J, van der Worp HB, de Borst GJ, Mali WP, Beard JD, Cleveland T, Engelter ST, Lyrer PA, Ford GA, Dorman PJ, Brown MM, International Carotid Stenting Study investigators. Long-term outcomes after stenting versus endarterectomy for treatment of symptomatic carotid stenosis: The International Carotid Stenting Study (ICSS) randomised trial. Lancet. 2015; 385:529–538. [PubMed: 25453443]

Bonnefous O, Luisy F, Kownator S. Arterial wall motion imaging: a new ultrasound approach to vascular characterisation. Medica Mundi. 2000; 44:37–43.

Brott TG, Hobson RW II, Howard G, Roubin GS, Clark WM, Brooks W, Mackey A, Hill MD, Leimgruber PP, Sheffet AJ, Howard VJ, Moore WS, Voeks JH, Hopkins LN, Cutlip DE, Cohen DJ, Popma JJ, Ferguson RD, Cohen SN, Blackshear JL, Silver FL, Mohr JP, Lal BK, Meschia JF, CREST Investigators. Stenting versus endarterectomy for treatment of carotid-artery stenosis. N Engl J Med. 2010; 363:11–23. [PubMed: 20505173]

Buerk DG, Goldstick TK. Arterial wall oxygen consumption rate varies spatially. Am J Physiol. 1982; 243:H948–H958. [PubMed: 7149047]

Burke GL, Evans GW, Riley WA, Sharrett AR, Howard G, Barnes RW, Rosamond W, Crow RS, Rautaharju PM, Heiss G. Arterial wall thickness is associated with prevalent cardiovascular disease in middle-aged adults. The Atherosclerosis Risk in Communities (ARIC) Study. Stroke. 1995; 26:386–391. [PubMed: 7886711]

Chen L, Low LK, DeLancey JO, Ashton-Miller JA. In vivo estimation of perineal body properties using ultrasound quasistatic elastography in nulliparous women. J Biomech. 2015; 48:1575–1579. [PubMed: 25801422]

Cheung CC, Yu AC, Salimi N, Yiu BY, Tsang IK, Kerby B, Azar RZ, Dickie K. Multi-channel pre-beamformed data acquisition system for research on advanced ultrasound imaging methods. IEEE Trans Ultrason Ferroelectr Freq Control. 2012; 59:243–253. [PubMed: 24626032]

Coli S, Magnoni M, Sangiorgi G, Marrocco-Trischitta MM, Melisurgo G, Mauriello A, Spagnoli L, Chiesa R, Cianflone D, Maseri A. Contrast-enhanced ultrasound imaging of intraplaque neovascularization in carotid arteries: Correlation with histology and plaque echogenicity. J Am Coll Cardiol. 2008; 52:223–230. [PubMed: 18617072]

Author Manuscript Author Manuscript Author Manuscript Author Manuscript

Comess KA, Choi JH, Xie Z, Achenbach S, Daniel W, Beach KW, Kim Y. Transthoracic coronary Doppler vibrometry in the evaluation of normal volunteers and patients with coronary artery stenosis. Ultrasound Med Biol. 2011; 37:679–687. [PubMed: 21497717]

De Andrade, DP. Interaction fluid structure on the laminar flow in curved pipes. Lisbon: Instituto Superior Tecnico; 2014.

De Fabritiis A, Conti E, Coccheri S. Management of patients with carotid stenosis. Pathophysiol Haemost Thromb. 2002; 32:381–385. [PubMed: 13679681]

Derdeyn CP, Chimowitz MI, Lynn MJ, Fiorella D, Turan TN, Janis LS, Montgomery J, Nizam A, Lane BF, Lutsep HL, Barnwell SL, Waters MF, Hoh BL, Hourihane JM, Levy EI, Alexandrov AV, Harrigan MR, Chiu D, Klucznik RP, Clark JM, McDougall CG, Johnson MD, Pride GL Jr, Lynch JR, Zaidat OO, Rumboldt Z, Cloft HJ, Stenting and Aggressive Medical Management for Preventing Recurrent Stroke in Intracranial Stenosis Trial Investigators. Aggressive medical treatment with or without stenting in high-risk patients with intracranial artery stenosis (SAMMPRIS): The final results of a randomised trial. Lancet. 2014; 383:333–341. [PubMed: 24168957]

Dunmire B, Beach KW, Labs K, Plett M, Strandness DE Jr. Cross-beam vector Doppler ultrasound for angle-independent velocity measurements. Ultrasound Med Biol. 2000; 26:1213–1235. [PubMed: 11120358]

Ekroll IK, Dahl T, Torp H, Løvstakken L. Combined vector velocity and spectral Doppler imaging for improved imaging of complex blood flow in the carotid arteries. Ultrasound Med Biol. 2014; 40:1629–1640. [PubMed: 24785436]

Ekroll IK, Swillens A, Segers P, Dahl T, Torp H, Lovstakken L. Simultaneous quantification of flow and tissue velocities based on multi-angle plane wave imaging. IEEE Trans Ultrason Ferroelectr Freq Control. 2013; 60:727–738. [PubMed: 23549533]

Feinstein SB. Contrast ultrasound imaging of the carotid artery vasa vasorum and atherosclerotic plaque neovascularization. J Am Coll Cardiol. 2006; 48:236–243. [PubMed: 16843169]

Feng B, Wang S, Li S, Yang X, Jiang ST. Experimental and numerical study on pressure distribution of 90° elbow for flow measurement. Sci Technol Nuclear Install (Iztok). 2014; 2014:964585.

Folkman J. Tumor angiogenesis: a possible control point in tumor growth. Ann Intern Med. 1975; 82:96–100. [PubMed: 799908]

Folkman J, Hochberg M. Self-regulation of growth in three dimensions. J Exp Med. 1973; 138:745–753. [PubMed: 4744009]

Folts J. Arterial blood pressure gradient across vulnerable plaque might increase rupture. J Am Coll Cardiol. 2007; 50:2440. [PubMed: 18154974]

Galis ZS, Lessner SM. Will the real plaque vasculature please stand up? Why we need to distinguish the vasa plaquorum from the vasa vasorum. Trends Cardiovasc Med. 2009; 19:87–94. [PubMed: 19679265]

Gardin JM, Bartz TM, Polak JF, O'Leary DH, Wong ND. What do carotid intima–media thickness and plaque add to the prediction of stroke and cardiovascular disease risk in older adults? The cardiovascular health study. J Am Soc Echocardiogr. 2014; 27:998–1005. [PubMed: 25172401]

Giannoni MF, Vicenzini E, Citone M, Ricciardi MC, Irace L, Laurito A, Scucchi LF, Di Piero V, Gossetti B, Mauriello A, Spagnoli LG, Lenzi GL, Valentini FB. Contrast carotid ultrasound for the detection of unstable plaques with neoangiogenesis: A pilot study. Eur J Vasc Endovasc Surg. 2009; 37:722–727. [PubMed: 19328729]

Glagov S, Weisenberg E, Zarins CK, Stankunavicius R, Kolettis GJ. Compensatory enlargement of human atherosclerotic coronary arteries. N Engl J Med. 1987; 316:1371–1375. [PubMed: 3574413]

Gössl M, Herrmann J, Tang H, Versari D, Galili O, Mannheim D, Rajkumar SV, Lerman LO, Lerman A. Prevention of vasa vasorum neovascularization attenuates early neointima formation in experimental hypercholesterolemia. Basic Res Cardiol. 2009; 104:695–706. [PubMed: 19458984]

Hansen-Smith F, Egginton S, Hudlicka O. Growth of arterioles in chronically stimulated adult rat skeletal muscle. Microcirculation. 1998; 5:49–59. [PubMed: 9702722]

Author Manuscript Author Manuscript Author Manuscript Author Manuscript

Hatsukami TS, Ross R, Polissar NL, Yuan C. Visualization of fibrous cap thickness and rupture in human atherosclerotic carotid plaque in vivo with high-resolution magnetic resonance imaging. Circulation. 2000; 102:959–964. [PubMed: 10961958]

Hlatky L, Hahnfeldt P, Folkman J. Clinical application of antiangiogenic therapy: Microvessel density, what it does and doesn't tell us. J Natl Cancer Inst. 2002; 94:883–893. [PubMed: 12072542]

Hoeks AP, Brands PJ, Smeets FA, Reneman RS. Assessment of the distensibility of superficial arteries. Ultrasound Med Biol. 1990; 16:121–128. [PubMed: 2183458]

Hoeks AP, Ruissen CJ, Hick P, Reneman RS. Transcutaneous detection of relative changes in artery diameter. Ultrasound Med Biol. 1985; 11:51–59. [PubMed: 3892817]

Hokanson DE, Mozersky DJ, Summer DS, Strandness DE. A phase-locked echo tracking system for recording arterial diameter changes in vivo. J Appl Physiol. 1972; 32:728–733. [PubMed: 5038866]

Housden RJ, Gee AH, Treece GM, Prager RW. Ultrasonic imaging of 3D displacement vectors using a simulated 2D array and beamsteering. Ultrasonics. 2013; 53:615–621. [PubMed: 23164173]

Huang X, Yang C, Canton G, Ferguson M, Yuan C, Tang D. Quantifying effect of intraplaque hemorrhage on critical plaque wall stress in human atherosclerotic plaques using three-dimensional fluid–structure interaction models. J Biomech Eng. 2012; 134:121004. [PubMed: 23363206]

Kartchner MM, McRae LP. Noninvasive evaluation and management of the "asymptomatic" carotid bruit. Surgery. 1977; 82:840–847. [PubMed: 929374]

Kartchner MM, McRae LP, Morrison FD. Noninvasive detection and evaluation of carotid occlusive disease. Arch Surg. 1973; 106:528–535. [PubMed: 4696726]

Kerwin WS, Oikawa M, Yuan C, Jarvik GP, Hatsukami TS. MR imaging of adventitial vasa vasorum in carotid atherosclerosis. Magn Reson Med. 2008; 59:507–514. [PubMed: 18306402]

Kim C, Yoon C, Park JH, Lee Y, Kim WH, Chang JM, Choi BI, Song TK, Yoo YM. Evaluation of ultrasound synthetic aperture imaging using bidirectional pixel-based focusing: Preliminary phantom and in vivo breast study. IEEE Trans Biomed Eng. 2013; 60:2716–2724. [PubMed: 23686939]

Knox R, Breslau P, Strandness DE. Quantitative carotid phonoangiography. Stroke. 1981; 12:798–803. [PubMed: 7303070]

Kucewicz JC, Dunmire B, Giardino ND, Leotta DF, Paun M, Dager SR, Beach KW. Tissue pulsatility imaging of cerebral vasoreactivity during hyperventilation. Ultrasound Med Biol. 2008; 34:1200–1208. [PubMed: 18336991]

Kucewicz JC, Dunmire B, Leotta DF, Panagiotides H, Paun M, Beach KW. Functional tissue pulsatility imaging of the brain during visual stimulation. Ultrasound Med Biol. 2007; 33:681–690. [PubMed: 17346872]

Lal BK, Beach KW, Sumner DS. Intracranial collateralization determines hemodynamic forces for carotid plaque disruption. J Vasc Surg. 2011; 54:1461–1471. [PubMed: 21820834]

Lees RS. Phonoangiography: Qualitative and quantitative. Ann Biomed Eng. 1984; 12:55–62. [PubMed: 6391302]

Lees RS, Dewey CF. Phonoangiography: A new noninvasive diagnostic method for studying arterial disease. Proc Natl Acad Sci USA. 1970; 67:935–942. [PubMed: 5289030]

Lenge M, Ramalli A, Boni E, Liebgott H, Cachard C, Tortoli P. High-frame-rate 2-D vector blood flow imaging in the frequency domain. IEEE Trans Ultrason Ferroelectr Freq Control. 2014; 61:1504–1514. [PubMed: 25167150]

Leung M, Yuan F, Menger MD, Boucher Y, Goetz AE, Messmer K, Jain RK. Angiogenesis, microvascular architecture, microhemodynamics, and interstitial fluid pressure during early growth of human adenocarcinoma LS174 T in SCID mice. Cancer Res. 1992; 52:6553–6560. [PubMed: 1384965]

Liebgott H, Basarab A, Gueth P, Cachard C, Delachartre P. Lateral RF image synthesis using a synthetic aperture imaging technique. IEEE Trans Ultrason Ferroelectr Freq Control. 2008; 55:2097–2103. [PubMed: 18986907]

Lima CO, Sahn DJ, Valdes-Cruz LM, Goldberg SJ, Barron JV, Allen HD, Grenadier E. Noninvasive prediction of transvalvular pressure gradient in patients with pulmonary stenosis by quantitative

Author Manuscript Author Manuscript Author Manuscript Author Manuscript

two-dimensional echocardiographic Doppler studies. Circulation. 1983; 67:866–871. [PubMed: 6825241]

Martini J, Honig CR. Direct measurement of intercapillary distance in beating rat heart in situ under various conditions of O_2 supply. Microvasc Res. 1969; 1:244–256. [PubMed: 5406306]

Maurice G, Wang X, Stoltz JF. Linear and nonlinear elastic modelling of the deformation of vasa vasorum. Clin Hemorheol Microcirc. 1998; 19:291–298. [PubMed: 9972666]

McCarthy MJ, Loftus IM, Thompson MM, Jones L, London NJ, Bell PR, Naylor AR, Brindle NP. Angiogenesis and the atherosclerotic carotid plaque: An association between symptomatology and plaque morphology. J Vasc Surg. 1999; 30:261–268. [PubMed: 10436445]

Nadkarni SK, Bilenca A, Bouma BE, Tearney GJ. Measurement of fibrous cap thickness in atherosclerotic plaques by spatiotemporal analysis of laser speckle images. J Biomed Opt. 2006; 11:021006. [PubMed: 16674181]

Nicolaides AN, Kakkos SK, Kyriacou E, Griffin M, Sabetai M, Thomas DJ, Tegos T, Geroulakos G, Labropoulos N, Doré CJ, Morris TP, Naylor R, Abbott AL, Asymptomatic Carotid Stenosis and Risk of Stroke (ACSRS) Study Group. Asymptomatic internal carotid artery stenosis and cerebrovascular risk stratification. J Vasc Surg. 2010; 52:1486–1496.e1–5. [PubMed: 21146746]

Papaioannou TG, Vavuranakis M, Androulakis A, Lazaros G, Kakadiaris I, Vlaseros I, Naghavi M, Kallikazaros I, Stefanadis C. In-vivo imaging of carotid plaque neoangiogenesis with contrast-enhanced harmonic ultrasound. Int J Cardiol. 2009; 134:e110–e112. [PubMed: 18495267]

Pastor-Barriuso R, Banegas JR, Damián J, Appel LJ, Guallar E. Systolic blood pressure, diastolic blood pressure, and pulse pressure: An evaluation of their joint effect on mortality. Ann Intern Med. 2003; 139:731–739. [PubMed: 14597457]

Pedley TJ, Luo XY. Modelling flow and oscillations in collapsible tubes. Theor Comput Fluid Dyn. 1998; 10:277–294.

Piechnik SK, Czosnyka M, Richards HK, Whitfield PC, Pickard JD. Cerebral venous blood outflow: A theoretical model based on laboratory simulation. Neurosurgery. 2001; 49:1214–1222. [PubMed: 11846915]

Pihler-Puzović D, Pedley TJ. Flutter in a quasi-one-dimensional model of a collapsible channel. Proc Math Phys Eng Sci. 2014; 470:201400.

Plett M, Beach KW. Ultrasonic vibration detection with wavelets: Preliminary results. Ultrasound Med Biol. 2005; 31:367–375. Erratum: 2006;32:1621–1622. [PubMed: 15749560]

Plett MI, Beach KW, Dunmire B, Brown KG, Primozich JF, Strandness E Jr. In vivo ultrasonic measurement of tissue vibration at a stenosis: A case study. Ultrasound Med Biol. 2001; 27:1049–1058. [PubMed: 11527591]

Rabben SI, Bjaerum S, Sorhus V, Torp H. Ultrasound-based vessel wall tracking: An auto-correlation technique with RF center frequency estimation. Ultrasound Med Biol. 2002; 28:507–517. [PubMed: 12049964]

Ramnarine KV, Hartshorne T, Sensier Y, Naylor M, Walker J, Naylor AR, Panerai RB, Evans DH. Tissue Doppler imaging of carotid plaque wall motion: a pilot study. Cardiovascular Ultrasound. 2003; 1:17. [PubMed: 14687422]

Redgrave JN, Gallagher P, Lovett JK, Rothwell PM. Critical cap thickness and rupture in symptomatic carotid plaques: The Oxford plaque study. Stroke. 2008; 39:1722–1729. [PubMed: 18403733]

Ricci S, Bassi L, Tortoli P. Real-time vector velocity assessment through multigate Doppler and plane waves. IEEE Trans Ultrason Ferroelectr Freq Control. 2014a; 61:314–324. [PubMed: 24474137]

Ricci S, Diciotti S, Francalanci L, Tortoli P. Accuracy and reproducibility of a novel dual-beam vector Doppler method. Ultrasound Med Biol. 2009; 35:829–838. [PubMed: 19110369]

Ricci S, Matera R, Tortoli P. An improved Doppler model for obtaining accurate maximum blood velocities. Ultrasonics. 2014b; 54:2006–2014. [PubMed: 24934798]

Ricci S, Vilkomerson D, Matera R, Tortoli P. Accurate blood peak velocity estimation using spectral models and vector Doppler. IEEE Trans Ultrason Ferroelectr Freq Control. 2015; 62:686–696. [PubMed: 25881346]

Ritman EL, Lerman A. The dynamic vasa vasorum. Cardiovasc Res. 2007; 75:649–658. [PubMed: 17631284]

Author Manuscript Author Manuscript Author Manuscript Author Manuscript

Saam T, Cai J, Ma L, Cai YQ, Ferguson MS, Polissar NL, Hatsukami TS, Yuan C. Comparison of symptomatic and asymptomatic atherosclerotic carotid plaque features with in vivo MR imaging. Radiology. 2006; 240:464–472. [PubMed: 16864672]

Schneiderman G, Mockros LF, Goldstick TK. Effect of pulsatility on oxygen transport to the human arterial wall. J Biomech. 1982; 15:849–858. [PubMed: 7161287]

Shamdasani V, Kim Y. Two-dimensional autocorrelation method for ultrasound-based strain estimation. Conf Proc IEEE Eng Med Biol Soc. 2004; 2:1380–1383. [PubMed: 17271950]

Shapiro, AH. Methods in hydraulics—Fluid mechanics, 16-mm sound films. The National Committee for Fluid Mechanics Films under a grant from the National Science Foundation: International Association for Hydro-Environment Engineering and Research Media Library, Educational Services; 1962. Pressure fields and flow acceleration.

Shaw R. The influence of hole dimensions on static pressure measurements. J Fluid Mech. 1960; 7:550–564.

Sikdar S, Beach KW, Vaezy S, Kim Y. Ultrasonic technique for imaging tissue vibrations: Preliminary results. Ultrasound Med Biol. 2005; 31:221–232. [PubMed: 15708462]

Sikdar S, Lee JC, Remington J, Zhao XQ, Goldberg SL, Beach KW, Kim Y. Ultrasonic Doppler vibrometry: Novel method for detection of left ventricular wall vibrations caused by poststenotic coronary flow. J Am Soc Echocardiogr. 2007; 20:1386–1392. [PubMed: 17764895]

Sommer G, Regitnig P, Költringer L, Holzapfel GA. Biaxial mechanical properties of intact and layer-dissected human carotid arteries at physiological and supraphysiological loadings. Am J Physiol Heart Circ Physiol. 2010; 298:H898–H912. [PubMed: 20035029]

Sun Z. Atherosclerosis and atheroma plaque rupture: Normal anatomy of vasa vasorum and their role associated with atherosclerosis. Sci World J. 2014; 2014:285058.

Takaya N, Yuan C, Chu B, Saam T, Polissar NL, Jarvik GP, Isaac C, McDonough J, Natiello C, Small R, Ferguson MS, Hatsukami TS. Presence of intraplaque hemorrhage stimulates progression of carotid atherosclerotic plaques: A high-resolution magnetic resonance imaging study. Circulation. 2005; 111:2768–2775. [PubMed: 15911695]

Takaya N, Yuan C, Chu B, Saam T, Underhill H, Cai J, Tran N, Polissar NL, Isaac C, Ferguson MS, Garden GA, Cramer SC, Maravilla KR, Hashimoto B, Hatsukami TS. Association between carotid plaque characteristics and subsequent ischemic cerebrovascular events: A prospective assessment with MRI–initial results. Stroke. 2006; 37:818–823. [PubMed: 16469957]

Tasinkevych Y, Klimonda Z, Lewandowski M, Nowicki A, Lewin PA. Modified multi-element synthetic transmit aperture method for ultrasound imaging: A tissue phantom study. Ultrasonics. 2013; 53:570–579. [PubMed: 23131337]

Teng Z, He J, Degnan AJ, Chen S, Sadat U, Bahaei NS, Rudd JH, Gillard JH. Critical mechanical conditions around neovessels in carotid atherosclerotic plaque may promote intraplaque hemorrhage. Atherosclerosis. 2012; 223:321–326. [PubMed: 22762729]

Teng Z, Sadat U, Brown AJ, Gillard JH. Plaque hemorrhage in carotid artery disease: Pathogenesis, clinical and biomechanical considerations. J Biomech. 2014; 47:847–858. [PubMed: 24485514]

Tortoli P, Lenge M, Righi D, Ciuti G, Liebgott H, Ricci S. Comparison of carotid artery blood velocity measurements by vector and standard Doppler approaches. Ultrasound Med Biol. 2015; 41:1354–1362. [PubMed: 25722028]

Treiman GS, McNally JS, Kim SE, Parker DL. Correlation of carotid intraplaque hemorrhage and stroke using 1.5 Tand 3 T MRI. Magn Reson Insights. 2015; 8(Suppl 1):1–8. [PubMed: 26056469]

Truijman MT, Kooi ME, van Dijk AC, de Rotte AA, van der Kolk AG, Liem MI, Schreuder FH, Boersma E, Mess WH, van Oostenbrugge RJ, Koudstaal PJ, Kappelle LJ, Nederkoorn PJ, Nederveen AJ, Hendrikse J, van der Steen AF, Daemen MJ, van der Lugt A. Plaque at Risk (PARISK): Prospective multicenter study to improve diagnosis of high-risk carotid plaques. Int J Stroke. 2014; 9:747–754. [PubMed: 24138596]

Underhill HR, Hatsukami TS, Fayad ZA, Fuster V, Yuan C. MRI of carotid atherosclerosis: Clinical implications and future directions. Nat Rev Cardiol. 2010; 7:165–173. [PubMed: 20101259]

Van Lammeren GW, den Hartog AG, Pasterkamp G, Vink A, de Vries JP, Moll FL, de Borst GJ. Asymptomatic carotid artery stenosis: Identification of subgroups with different underlying plaque characteristics. Eur J Vasc Endovasc Surg. 2012; 43:632–636. [PubMed: 22507923]

Author Manuscript Author Manuscript Author Manuscript Author Manuscript

Wang X, Li X. Biomechanical behaviors of curved artery with flexible wall: A numerical study using fluid–structure interaction method. Comput Biol Med. 2011; 41:1014–1021. [PubMed: 21943789]

Whereat AF. Oxygen consumption of normal and atherosclerotic intima. Circ Res. 1961; 9:571–575. [PubMed: 13784778]

Whereat AF. Recent advances in experimental and molecular pathology; Atherosclerosis and metabolic disorders in the arterial wall. Exp Mol Pathol. 1967; 7:233–247. [PubMed: 4383229]

Yoshida K, Fukumitsu R, Kurosaki Y, Funaki T, Kikuchi T, Takahashi JC, Takagi Y, Yamagata S, Miyamoto S. The association between expansive arterial remodeling detected by high-resolution MRI in carotid artery stenosis and clinical presentation. J Neurosurg. 2015; 13:1–7.

Yuan C, Zhang SX, Polissar NL, Echelard D, Ortiz G, Davis JW, Ellington E, Ferguson MS, Hatsukami TS. Identification of fibrous cap rupture with magnetic resonance imaging is highly associated with recent transient ischemic attack or stroke. Circulation. 2002; 105:181–185. [PubMed: 11790698]

Zahiri-Azar R, Goksel O, Yao TS, Dehghan E, Yan J, Salcudean SE. Methods for the estimation of sub-sample motion of digitized ultrasound echo signals in two dimensions. Conf Proc IEEE Eng Med Biol Soc. 2008; 2008:5581–5584. [PubMed: 19163982]

Zahnd G, Boussel L, Marion A, Durand M, Moulin P, Serusclat A, Vray D. Measurement of two-dimensional movement parameters of the carotid artery wall for early detection of arteriosclerosis: A preliminary clinical study. Ultrasound Med Biol. 2011; 37:1421–1429. [PubMed: 21816288]

Zarins CK, Weisenberg E, Kolettis G, Stankunavicius R, Glagov S. Differential enlargement of artery segments in response to enlarging atherosclerotic plaques. J Vasc Surg. 1988; 7:386–394. [PubMed: 3346952]

Zetting O, Hennersperger C, Zu Berge CS, Baust M, Navab N. 3D velocity field and flow profile reconstruction from arbitrarily sampled Doppler ultrasound data. Med Image Comput Computer-Assisted Interv. 2014; 17(Pt 2):611–618.

Zhou Z, Li R, Zhao X, He L, Wang X, Wang J, Balu N, Yuan C. Evaluation of 3D multi-contrast joint intra- and extracranial vessel wall cardiovascular magnetic resonance. J Cardiovasc Magn Reson. 2015; 17:41. [PubMed: 26013973]

Zierler RE, Beach KW, Bergelin RO, Lal BK, Moore WS, Roubin GS, Voeks JH, Brott TG, CREST Investigators. Agreement between sitereported and ultrasound core laboratory results for duplex ultrasound velocity measurements in the Carotid Revascularization Endarterectomy versus Stenting trial. J Vasc Surg. 2014; 59:2–7. [PubMed: 24055515]

Author Manuscript Author Manuscript Author Manuscript Author Manuscript

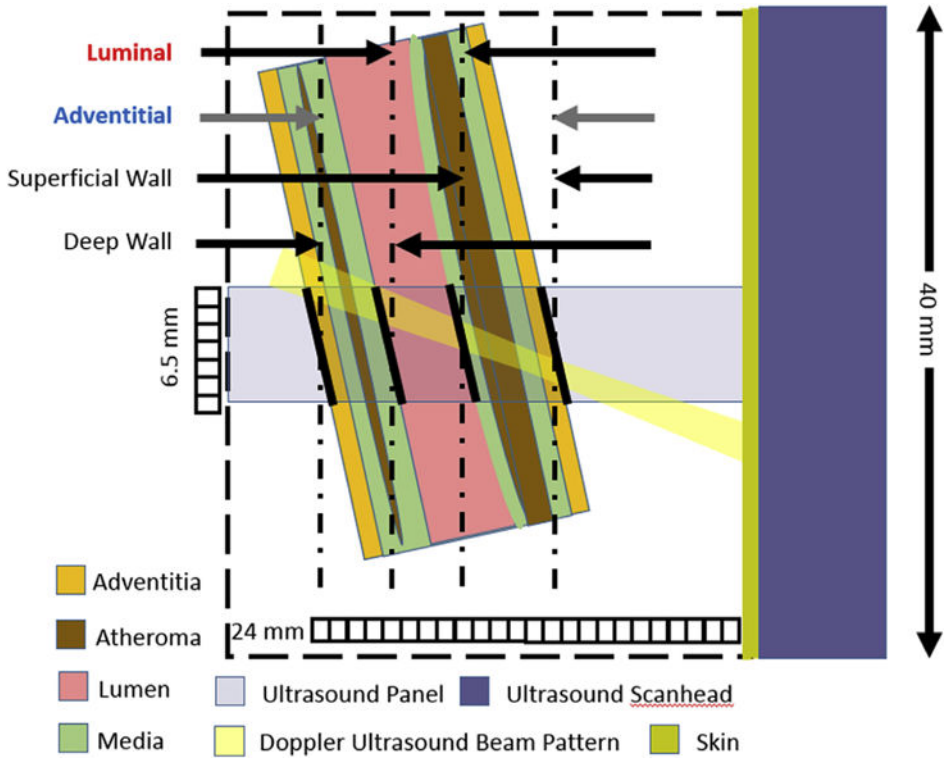

Fig. 1.

Ultrasound system for wall motion measurement. Three ultrasound beam patterns are used for data acquisition from the linear array scanhead. *Dashed outline*: conventional 2-D B-mode pilot image, 40 mm high. *Light blue panel*: scan pattern 6.5 mm high, 16 lines at 270 frames per second for acquisition of wall motions. *Yellow angled beam pattern*: Doppler beam, tilted 20° from B-mode lines. Between-frame panel motion data were obtained for each of the four interfaces: superficial adventitial, superficial intimal, deep intimal and deep adventitial. Interface locations were outlined by the sonographer. With the radiofrequency data from 16 lines in the panel at each marked depth, a displacement waveform with depth displacement resolution of 0.0001 mm was created. The frame-to-frame displacements were summed for each interface to provide a position-versus-time waveform for each interface. Luminal and adventitial diametric waveforms and superficial and deep wall waveforms were computed by taking the respective differences of the positional waveforms.

Author Manuscript Author Manuscript Author Manuscript Author Manuscript

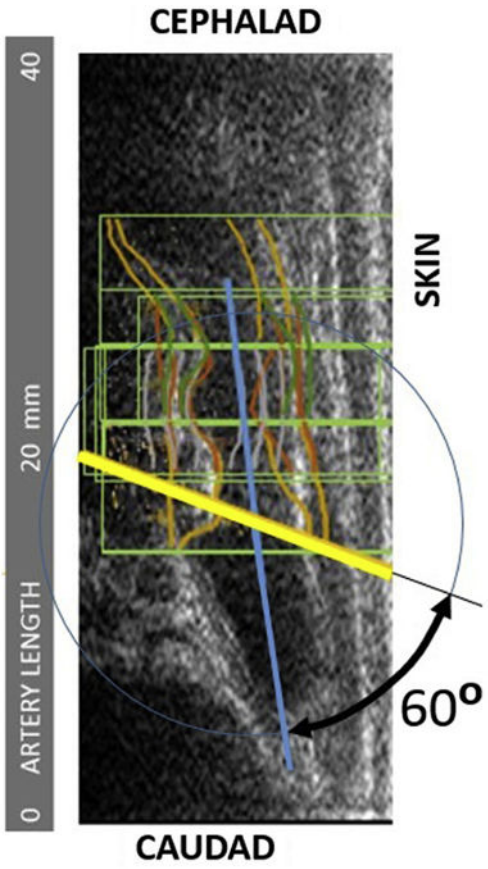

Fig. 2.

Pilot image with six panels and interface outlines. Pilot image oriented with top = cephalad, bottom = caudad, right = skin. *Six green boxes* = 6 panels where 16 line panels of radiofrequency data were acquired on this artery. *Various colored curving lines* = intimal and adventitial walls traced by the sonographer in each panel. *Yellow line* = Doppler beam pattern at the location of highest velocity. *Blue line* = artery axis. *Black arc* = 60° Doppler angle between blue and yellow lines. The *gray color stripe* represents the dimensional scale along the artery (mm).

Author Manuscript Author Manuscript Author Manuscript Author Manuscript

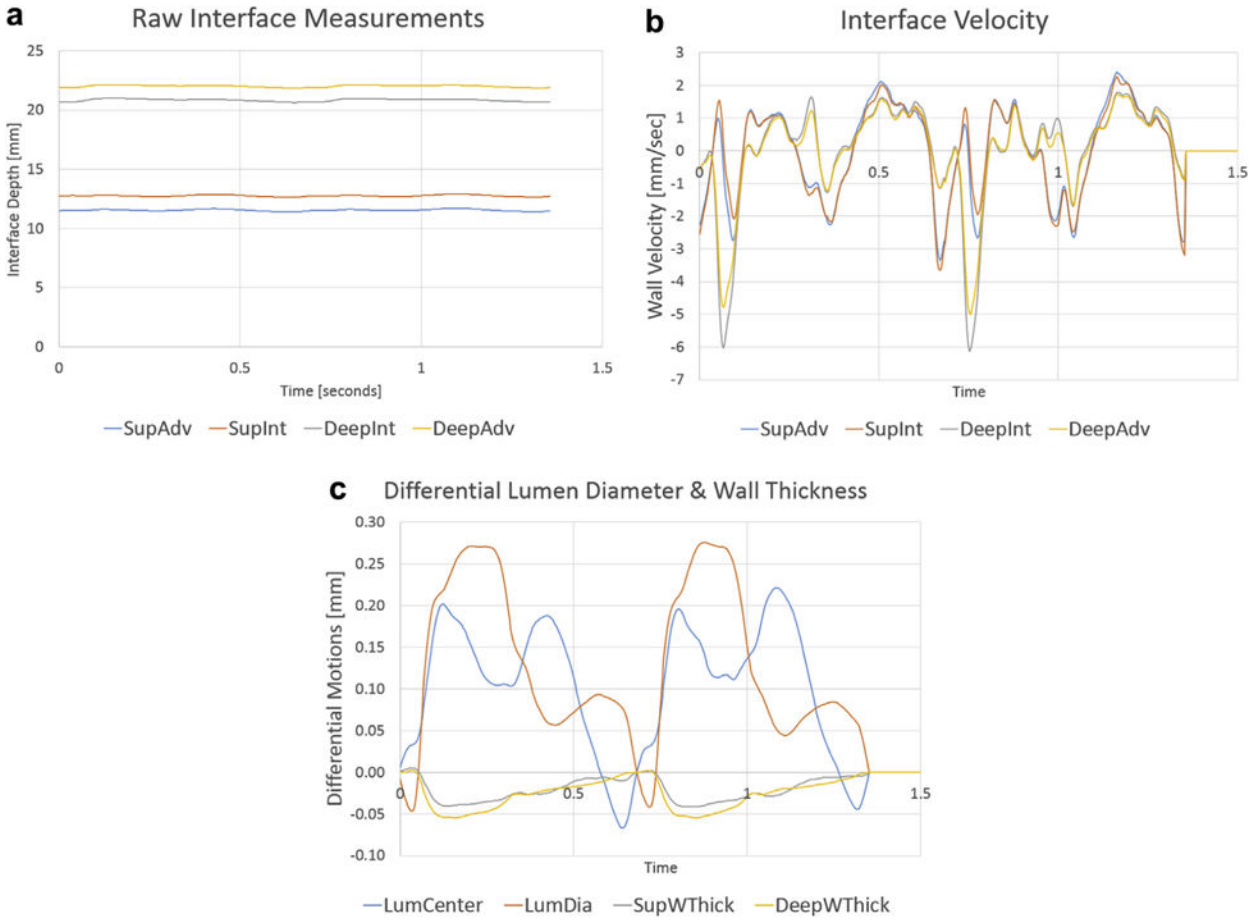

Fig. 3.

Waveform processing steps in a normal artery. (a) Interface waveforms illustrating small displacements compared with depth. (b) Interface velocities illustrating reproducibility between cardiac cycles. Note the similarity between the superficial adventitial and superficial intimal waveforms and the similarity between the deep adventitial and deep intimal waveforms. (c) Lumen center, lumen diametric and both wall thickness motion waveforms. Lumen center (LumCentr) = (DeepInt+SupInt)/2. Lumen diameter (LumDia) = (DeepInt−SupInt). Superficial wall thickness (SupWThick) = (SupInt−SupAdv). Deep wall thickness (DeepWThick) = (SupAdv−SupInt). The lumen diameter waveform (*orange*) indicates a diameter decrease of 0.047 mm at 33 ms after the QRS, with a maximum increase to +0.276 mm at 207 ms. The two wall thickness waveforms illustrate expected decreases at 130 ms of 0.040 mm (superficial wall) and 0.054 mm (deep wall). The waveform of the lumen center (*blue*) illustrates a different morphology. This center waveform can be used to compute the differential wall pressure between the superficial and deep walls; the differential wall pressure is combined with the Bernoulli pressure depression to determine the net wall pressure.

Author Manuscript Author Manuscript Author Manuscript Author Manuscript

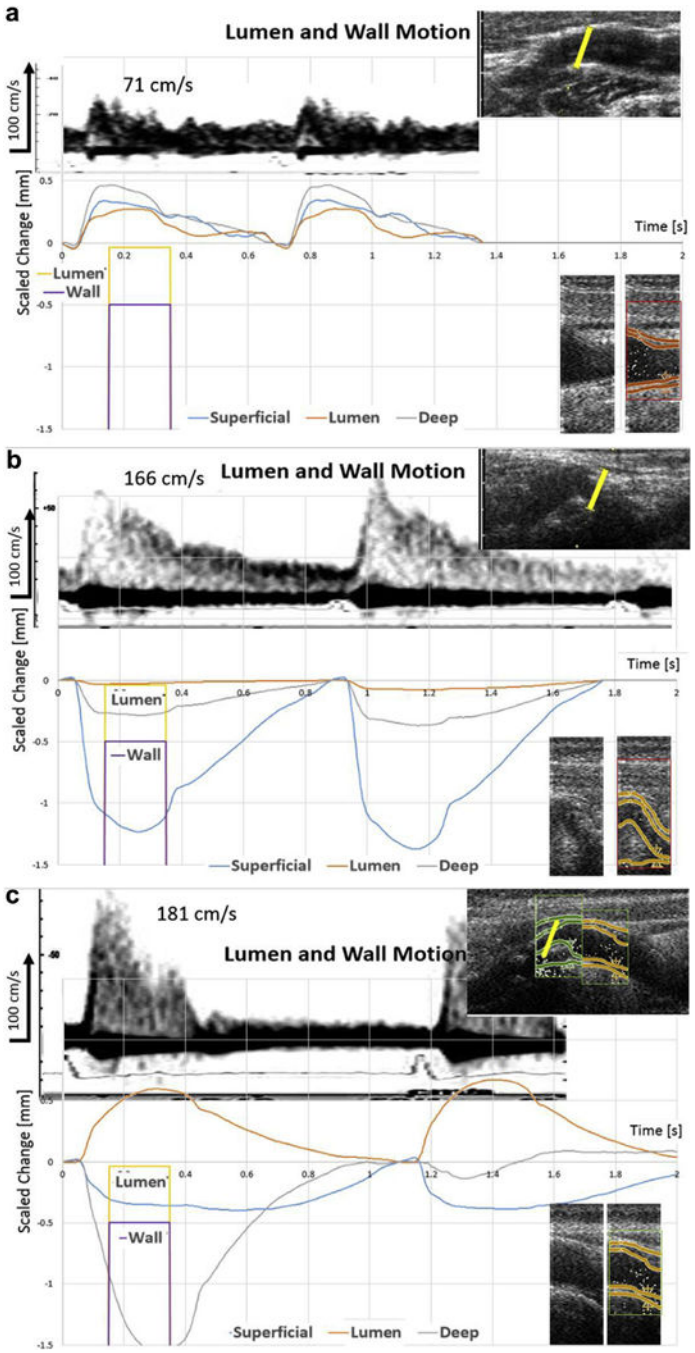

Fig. 4.

Spectral Doppler blood velocity with diametric and scaled wall thickness waveforms. Upper right: 2-D B-mode pilot image with *yellow* Doppler line. Upper left: Spectral waveform with angle-adjusted peak systolic blood velocity. The spectral Doppler waveforms in all three figures have the same velocity scale. The *arrow* indicates the Doppler shift equivalent to 100 cm/s angle-adjusted velocity. Lower right: Duplicated pair of 2-D B-mode panels illustrating the demodulated radiofrequency data. The left panel is not obstructed by the outlines. The right panel has superimposed lines illustrating outlined anatomic interfaces. The *orange*

Author Manuscript Author Manuscript Author Manuscript Author Manuscript

wave indicates diameter change (mm); *blue wave*, scaled superficial wall thickness change (* –diameter/thickness) (mm); *gray wave*, scaled deep wall thickness change (* –diameter/thickness) (mm); *yellow line*, Doppler sample volume; *yellow box*, threshold for systolic diametric lumen diametric reduction (−0.05 mm); *purple box*, threshold for scaled wall thickness inflation (−0.5 mm). The time scales in all waveforms are aligned. (a) 71 cm/s: Normal diametric wall thickness waveforms revealing similar amplitudes. (b) 166 cm/s: Systolic luminal diametric reduction plus superficial wall increase. (c) 181 cm/s: Extreme luminal expansion (>0.5 mm) plus deep wall increase.

Author Manuscript Author Manuscript Author Manuscript Author Manuscript

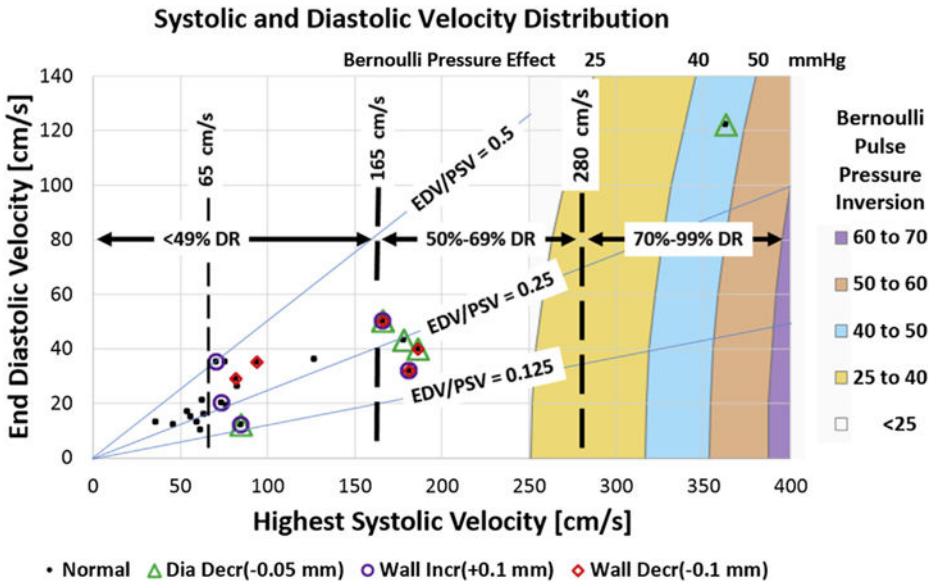

Fig. 5.

Highest systolic and diastolic Doppler velocities for each artery. *Dashed lines*: thresholds for stenosis severity = 165 and 280 cm/s. Empirical threshold for expected waveforms = 65 cm/s. *Color stripes*: systolic and diastolic intrastenotic Bernoulli pressure pulse modulation. *Orange stripe*: velocity range with a Bernoulli pulse pressure modulation of 25–40 mm Hg. *Blue stripe*: velocity range with a Bernoulli pulse pressure modulation of 40–50 mm Hg. *Pink stripe*: velocity range with a Bernoulli pulse pressure modulation of 50–60 mm Hg. *Purple stripe*: velocity range with a Bernoulli pulse pressure modulation >60 mm Hg. *Black dot*: highest systolic and diastolic velocity in each artery. *Green triangle*: arteries with panels illustrating systolic luminal diametric decrease. *Purple circle*: arteries with panels illustrating systolic wall thickness increase. *Red diamond*: arteries with panels illustrating systolic wall thickness decrease. In all arteries, at least one proximal panel had normal waveforms. A single artery might exhibit one abnormality in one panel at one location and a different abnormality in another panel at another location. A single panel might reveal a thickness decrease on one wall and thickness increase on the other (one case). For each artery, all abnormal waveform shapes are marked around the point indicating the highest systolic and diastolic velocities.

Author Manuscript Author Manuscript Author Manuscript Author Manuscript

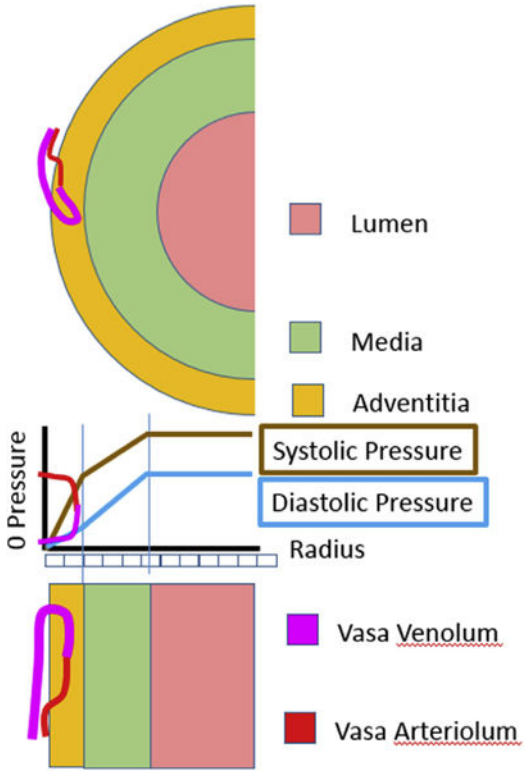

Fig. 6.

Monotonic systolic and diastolic pressure profiles in adventitia and media. Pressure outside the artery is atmospheric; pressure inside the artery lumen is systolic or diastolic. The pressure gradient through the adventitia (*gold*) and media (*green*) is monotonic, increasing from surface to lumen. The normal avascular media may have incompressible elastic properties. In contrast, the normal adventitia is perforated with high-pressure pulsating vasa-arterioles and low pressure vasa-venules on a sub-resolution scale (<0.1 mm), which foster changes in volume by a few percent (venular volume) at low pressures and pulsations by up to 1% (arteriolar volume) at all pressures below arteriolar systole. The pressure gradient in the wall in the radial direction varies with luminal pressure from a proportion of systolic to a proportion of diastolic systemic pressure depending on the composite elastic and hysteresis tissue properties (Sommer et al. 2010). These properties are different in live tissues with inflated microvessels compared with excised tissues.

Author Manuscript Author Manuscript Author Manuscript Author Manuscript

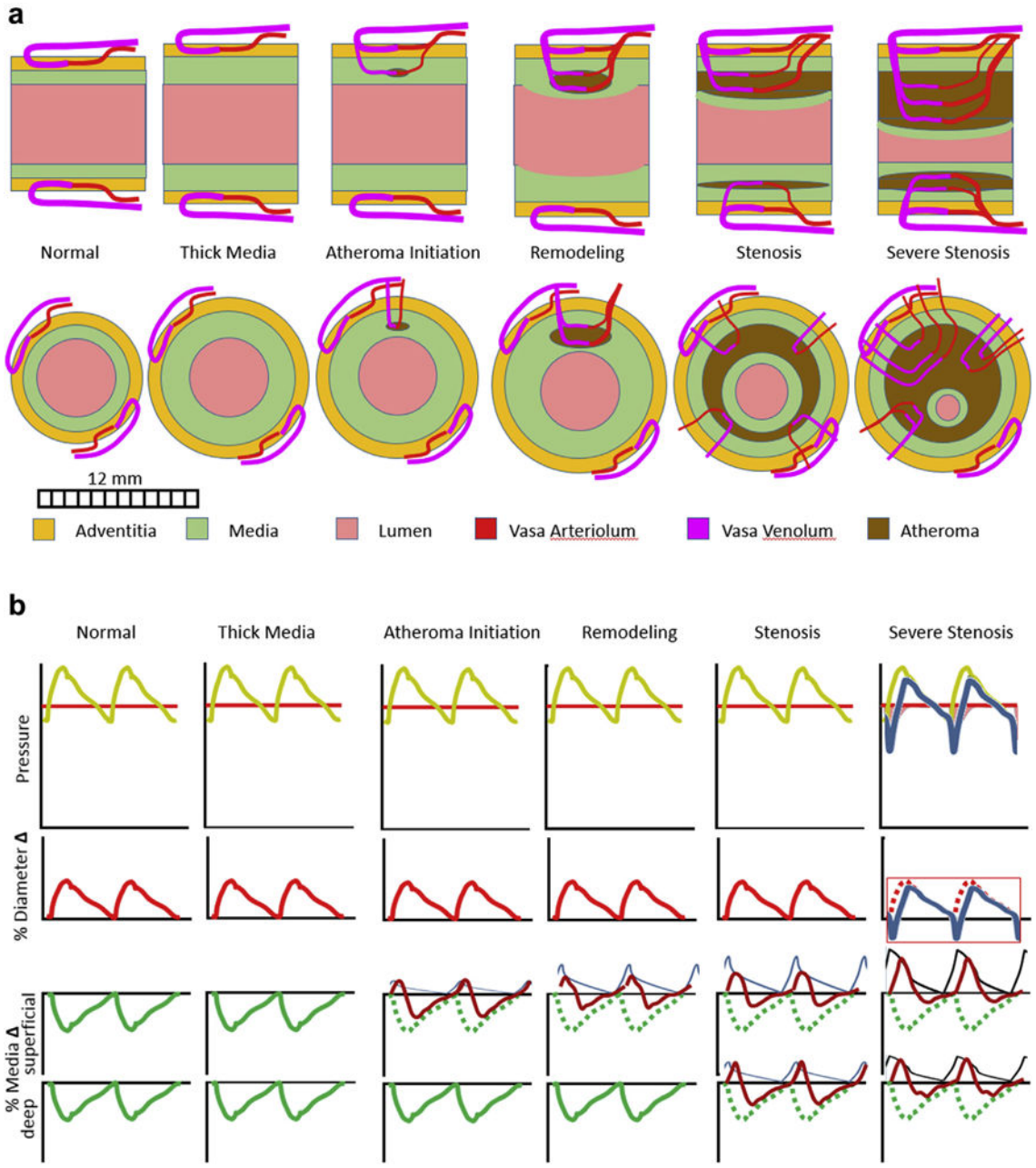

Fig. 7.

(a) Stages of atheroma development. Atheroma initiation cannot occur without the formation of neovascular vasa plaquorum to provide nourishment to the atheroma. The atheroma grows over time both circumferentially and longitudinally. The pressure in the vasa arteriolum is near the mean of arterial pressure, providing a positive perfusion pressure, at least during systole, with intermittent flow through the vasa venolum returning blood to adjacent major veins. When the atheroma fully embraces the artery (Fig. 3 in Zarins et al. 1988), then expansive remodeling of the adventitia ceases; further atheroma growth or expansion impinges on the lumen, causing stenosis. (b) Pulsatile expansion of the artery wall due to filling and emptying of vasa vasorum. Columns 1 and 2: Incompressible avascular

Author Manuscript Author Manuscript Author Manuscript Author Manuscript

elastic media becomes thinner during systole as the artery circumference increases in proportion to diameter increases. Additional pulsation in the vascularized adventitia caused by filling and emptying of vasa vasorum may also contribute; but the adventitial thickness is small (0.25 mm) compared with that of the media and can be spatially resolved. Columns 3–5: increasing volume fraction of vasa plaquorum within the media, filling in systole and emptying in diastole as it does in the myocardium (Ashikawa et al. 1986). Column 6: interstenotic Bernoulli luminal pressure depression allows blood to flow into the atheroma vasa plaquorum during high systolic intrastenotic luminal velocity. Upper row: *gold curves*—arterial supply pressure; *blue curve*—arterial pressure minus intrastenotic Bernoulli pressure depression. Middle row: *red curves*—percentage expansion of the arterial diameter; *blue curve*—percentage expansion at the site of the stenosis. Lower two rows: *green curves*—percentage change in wall thickness; *blue curve*—change in composite neovascular medial tissue thickness; *brown curves*—combined change in wall thickness expected in this study. *Dotted curves* are reference curves.

Author Manuscript Author Manuscript Author Manuscript Author Manuscript

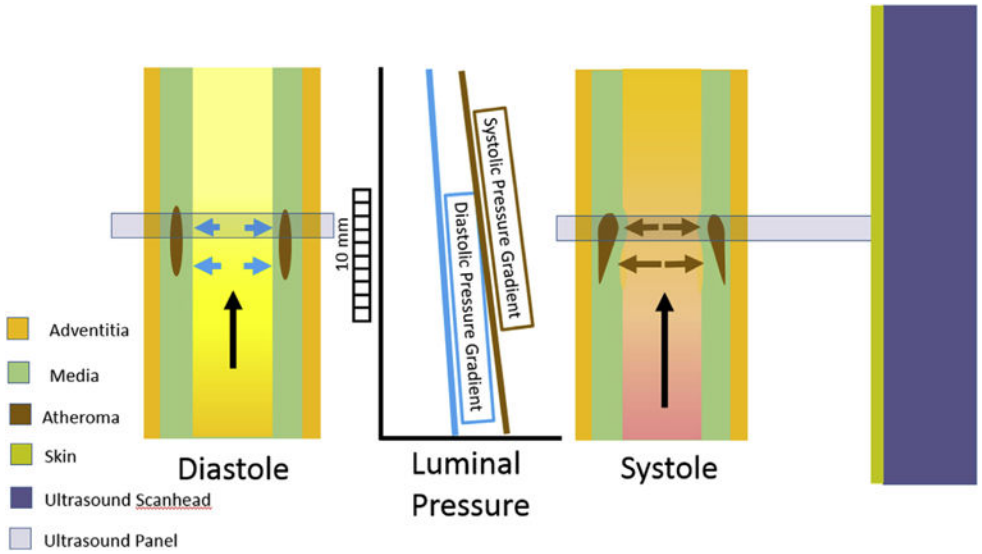

Fig. 8.

Theoretical longitudinal atheroma distortion by luminal pressure gradient. A liquefied atheroma core, whether lipid or hemorrhage, will exhibit cyclic shape distortion. Flow along the artery causes a longitudinal pressure gradient that is proportional to the wall shear stress. The gradient is higher in systole than diastole, when the velocity is greater, causing a cyclic distortion. Even if this pressure gradient is small, the liquid atheromatous core will flow from the region of higher pressure to that of lower pressure, bulging into the more distal arterial lumen. Of course, the distal bulge into the lumen will alter luminal flow, exacerbating the pressure gradient and, thus, causing longitudinal shear stress on the distorted atheroma. This stress is superimposed on the other stresses, further increasing the strain. The detection of such surface distortions requires a 2-mm-wide panel resolution to differentiate the distal bulge from the proximal retraction.

Author Manuscript Author Manuscript Author Manuscript Author Manuscript

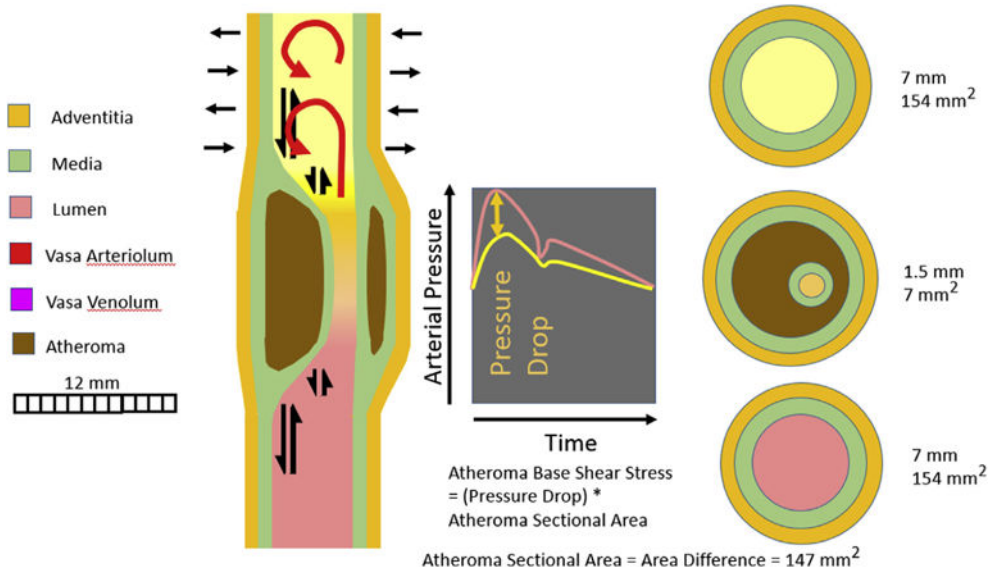

Fig. 9.

Theoretical longitudinal shear forces applied to atheroma. Left: longitudinal section through atheromatous stenosis. Center: luminal blood pressure waveform proximal (*salmon*) and distal (*yellow*). Right: arterial cross sections; upper = distal, lower = proximal. Note the pressure waveform time delay between proximal and distal locations and the peak pressure difference combine to create a longitudinal pressure drop. The pressure drop is balanced by the shear stress within the atheroma. Atheroma shear force = area difference (147 mm^2) × pressure drop.

Author Manuscript Author Manuscript Author Manuscript Author Manuscript

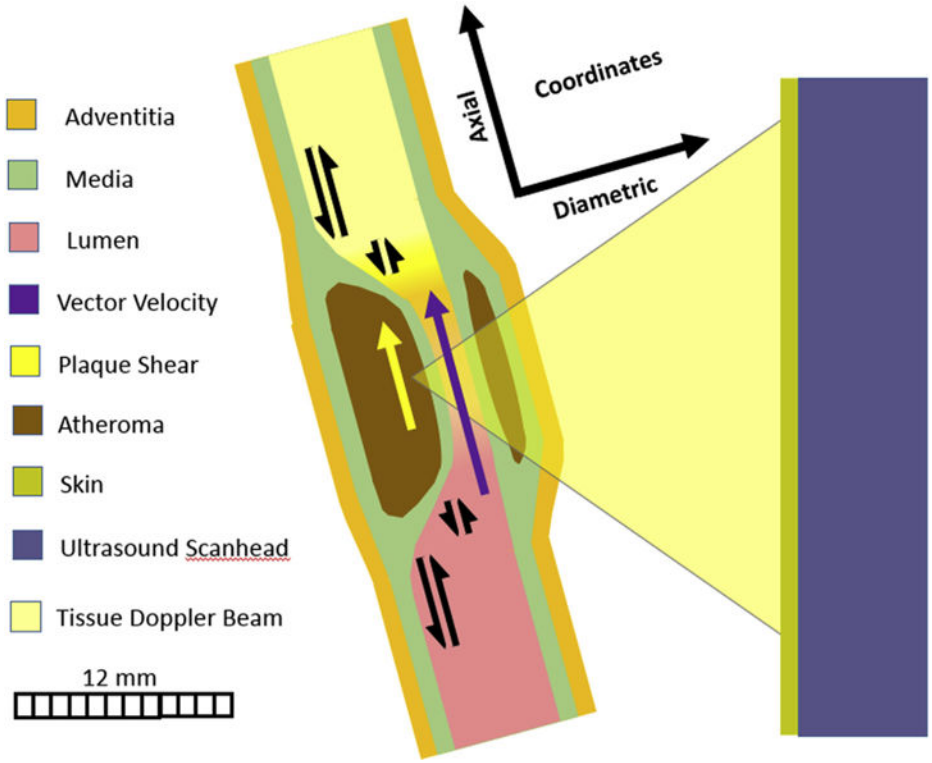

Fig. 10.

Wide-aperture ultrasound configuration used to measure 2-D arterial strains. Both diametric and axial strains should be measured for a complete documentation of atheroma mechanics. The wide aperture also allows vector Doppler of the blood flow. The Doppler measurement should include three separate velocity waveform measurements: (i) the highest velocity for use in computing the Bernoulli pressure depression, (ii) velocity stream line curvature to derive the axial displacement forces and differential wall pressures between superficial and deep walls to be added to the Bernoulli pressure depression and (iii) cross-axial velocity oscillations up to 500 Hz to characterize the power-dissipating, post-stenotic turbulence associated with the pressure drop across the stenosis.

Author Manuscript Author Manuscript Author Manuscript Author Manuscript

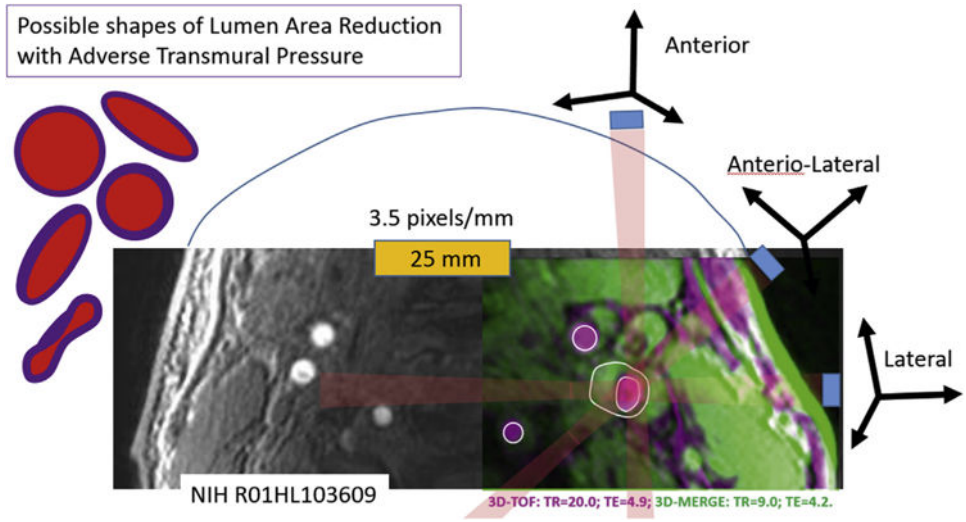

Fig. 11.

Colorized composite magnetic resonance imaging (MRI) dual-sequence image of carotid diametric reduction axes and recommended examination angles of approach for a complete evaluation by ultrasound. Left: Different possible modes of arterial cross-sectional area change. Right: Alternative ultrasound approaches to longitudinal imaging of the carotid artery. Atheroma is outlined in *white*. In this case, the atheroma (*green*) is limited to the medial wall. Although the atheroma volume is considerable, the lumen (*pink*) is not diminished in cross-sectional area. The atheroma has not yet embraced the lumen circumference, so a stenosis is not present. *Pink*: 3-D MRI 3-D TOF sequence—TR = 20.0, TE = 4.9. *Green*: MRI 3-D MERGE sequence—TR = 9.0, TE = 4.2. *Light blue rectangles*: locations of ultrasound scan-head for 3 recommended views, *black arrows*: coordinates of ultrasound images, *salmon color*: ultrasound beam planes.

Author Manuscript

Author Manuscript

Author Manuscript

Author Manuscript

Table 1

Carotid artery examination data requirements versus ultrasound and MR capability

	Requirement	Capability	
Characteristic	**Atheroma**	**Ultrasound**	**MRI**
Radial resolution, cap (mm)			
2-D MRI	0.05* +	0.2	0.39
3-D MRI	0.05* +	0.2	0.625
Displacement resolution (mm)	0.001	0.0001	0.55
Time resolution (ms)			
Expansion (ms)	40 (24 Hz)	0.01	50
Bruit	0.5 (500 Hz)	0.01	50
3-D volume reproducibility error (%)		6–15	10
Dimensional co-registration (mm)	2	4	0.7
Tissue identification			
Calcium		Yes	Yes
Fibrous		High GSM	Yes
Hemorrhage		Low GSM	Yes
Lipid/necrosis			Yes
Flow lumen identification		Yes	Yes

MRI = magnetic resonance imaging; GSM = gray-scale median of the atheroma on ultrasound imaging (Biasi et al. 1999).

*Atheroma cap thickness (Hatsukami et al. 2000; Nadkarni et al. 2006).